8-2015

# Macro model for solid and perforated masonry infill shear walls.

Farid Nemati
*University of Louisville*

# MACRO MODEL FOR SOLID AND PERFORATED
# MASONRY INFILL SHEAR WALLS

By

Farid Nemati
B. S., IAU, 2006
M. Sc., IUST, 2010

A Dissertation
Submitted to the Faculty of the
J. B. Speed School of Engineering
University of Louisville
in Partial Fulfillment of the Requirements
for the Degree of

Doctor of Philosophy

in Civil Engineering

Civil and Environmental Engineering Department
University of Louisville
Louisville, KY

August 2015

# MACRO MODEL FOR SOLID AND PERFORATED

# MASONRY INFILL SHEAR WALLS

By

Farid Nemati
B. S., IAU, 2006
M. Sc., IUST, 2010

A Dissertation Approved on

July 24<sup>th</sup>, 2015

By the Following Dissertation Committee

_____

Dr. William M. McGinley

_____

Dr. Thomas D. Rockaway

_____

Dr. Roger D. Bradshaw

_____

Dr. Young Hoon Kim

This Dissertation is dedicated to my wife Neda, and to all of the people who helped me finish this work.

# ACKNOWLEDGEMENTS

# ABSTRACT

## MACRO MODEL FOR SOLID AND PERFORATED MASONRY INFILL SHEAR WALLS

Farid Nemati

July 7, 2015

In this dissertation the performance of masonry walls enclosed by frame structures is studied and a new finite element model for these systems is presented. As part of this effort, the common modeling approaches i.e. micro-models and macro-models are briefly reviewed and their specifications are compared. Based on the findings in these comparisons, it was shown that macro modeling is the preferred modeling approach and the development of the new model is presented. The proposed model is described in detail and the calibration procedures along with the material models, used in the proposed model, are presented. To account for the interaction of the frame and the shear wall a contact member is developed. In support of this development three of most common solutions for contact problems that can be also used in modeling the frame-infill interaction problem are described; a detailed description for the chosen method along with a simple structural example is given.

A method for capturing the behaviors of the steel reinforcement (if present) is presented for the case where the infill shear walls are reinforced.

The proposed element was examined to see if it passes a patch test.

Finally, a number of experimental tests conducted by other researchers are modeled using the proposed model and the results are compared with the behavior predicted by the model. Good agreement between the predicted and measured behavior was achieved.

## TABLE OF CONTENTS

# LIST OF TABLES

## LIST OF FIGURES

# CHAPTER 1: INTRODUCTION

Many of the pre-1950 constructed buildings in the United States are frame-type structures with enclosed brick or concrete masonry walls in their perimeter portals. As an example, about 40 % of the buildings inventoried by U.S. Army have been classified as concrete frames enclosing infill shear walls, while this structural system has shown to be vulnerable to seismic damage [Bashandy et al., 1995]. In addition, newer construction has also used similar systems in South and Central America, North Africa and Southern Europe. Unless these structural systems are designed to avoid any considerable interaction with the surrounding frame, the wall usually participates in the performance of the structure, under lateral loadings, i.e. seismic or wind loads. The non-participating walls are not studied here as potential structural elements, and the study here is limited to the participating enclosed walls also known as infill walls. From this point in this study, the term infill wall refers to the participating infill walls.

The infill walls can significantly alter the stiffness and strength of the surrounding frame; especially under lateral loadings, the infill wall increases the stiffness of the combined structural system leading to a reduction in the natural period of the structural system and its ductility [El-Dakhakhni 2003]. The infill wall can also cause pre-mature failure of the frame elements in the cases where the infill wall imparts large shear loads to the surrounding frame [FEMA 178, 1992]. Thus, accurate study of the frame-wall interaction is of great importance and neglecting the infill wall participation in design may be unsafe [Asteris 2011].

1

To assess the performance of infill walls, many computational models have been created and many experimental tests have been conducted in the past sixty years. Each of these methods has been applied to the analysis and design of masonry infill shear walls with varying degrees of success.

The objectives of the following investigation was to evaluate the current state of the art for the analysis masonry infill shear walls, identify where the current state of the art is lacking, develop an analytical model that can be used to accurately predict the performance of masonry in-fill shear walls; unreinforced, reinforced and with openings, but is simple enough to use to support the assessment and rehabilitation of existing buildings and the design of new structures.

In the following section, a literature review of the current state of the art is presents. Chapter 2 presents the detailed model development and Chapter 3 present the procedures used to develop the material stress-strain relationships and calibrate the model. Chapter 4 presents a discussion of the model results when compared with measured unreinforced and reinforced masonry infill shear walls performance, with and without openings. A discussion of the effects of openings on the performance of the masonry infill shear walls is also presented in this chapter. Chapter 5 provides a summary, conclusions and recommendations.

## Literature Review

To assess the performance of masonry infill shear walls, a number of computational models have been created and numerous experimental tests have been conducted in the past sixty years. The data from the experimental tests were used to evaluate the theoretical models proposed by various researchers or to update the design

codes/standards, for such structural systems. The following section of this document will describe this in more detail.

In general, the computational models proposed hitherto, can fall into two general groups: micro-models and macro-models. In micro-models, the wall parts, i.e. the units and mortar are usually considered as two separate element types and the interface between them may also be modeled as third type of element [Lourenço et al. 2006]. In contrast, the macro-elements consider the units, mortar and the interface between them as a homogeneous isotropic/anisotropic material [Lourenço et al. 2006]. The merged material model assumed in macro-models can be either isotropic or anisotropic based on the focus of study and desired precision. These modeling approaches along with their general specifications will be briefly described later in this work.

**Micro-models:**

One of the main modeling approaches for assessing the behavior of infill walls under loading is to use micro-models. Micro-models can fall into two general groups, i.e. simplified and detailed. Although the basic idea behind the two groups may seem very similar, the required computational effort and achieved accuracy of the results can vary significantly [Lourenço, 2006].

In detailed micro-models, separate continuum elements describe units and mortar at the location of joints but the unit-mortar interface elements are discontinuous. In the simplified micro-modeling each unit and the surrounding mortar joint are represented by continuum elements, also known as expanded units, while the unit-mortar interface is lumped into discontinuous elements at mid-thickness of the mortar layers [Lourenço et al. 2006] and [Grecchi 2010]; see Fig. 1 taken from [Lourenço, 2006].

3
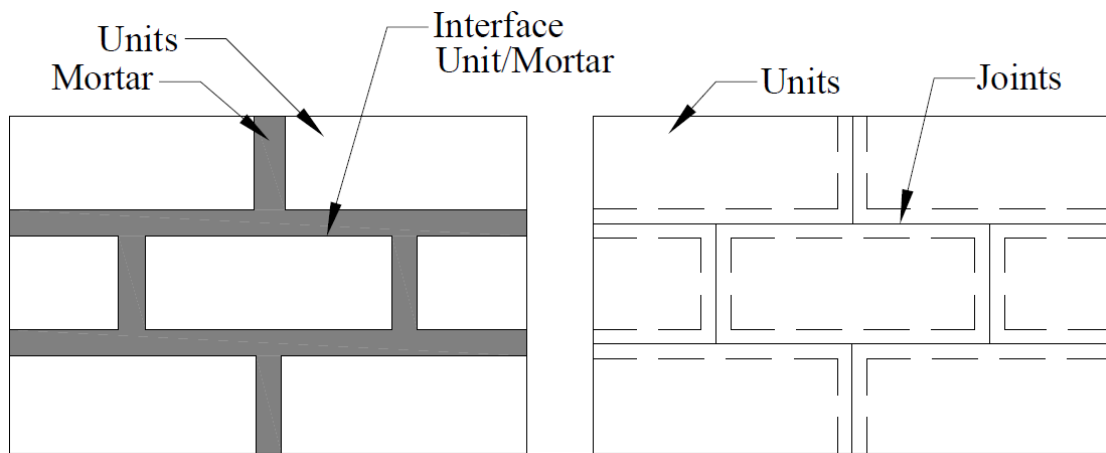
Figure 1. 1. Micro-Modeling Strategies for Masonry (a) Detailed Micro-Modeling; (b) Simplified Micro-Modeling [taken from Lourenço, 2006]

In detailed micro-models, the material properties of units and mortar must be defined separately. In addition, the unit-mortar interface is considered as a separate plane with potential crack/slip [Lourenço et al. 2006]. The detailed micro-modeling approach has shown to be very accurate for analyzing the local behavior of infill walls both in linear elastic and nonlinear/inelastic zones [Grecchi, 2010].

On the other hand, the simplified micro-models can be only used when the material is experiencing linear deformations. This is mostly because of the large ratio of unit stiffness to mortar stiffness that induces significant inaccuracies when the wall is showing nonlinear behavior [Zucchini and Lourenço, 2002].

Thus, to assess the nonlinear behavior of masonry walls and achieve sufficiently accurate results, very fine meshes must be used along with detailed micro-models [Zucchini et al. 2002]; this modeling approach requires a significant computational effort. In addition, the location of units and thicknesses of mortar layers places constraints on the finite element mesh generation procedure. This is especially important when the wall is perforated, where additional considerations on mesh generation must be made to reflect the pattern of units and mortar around the

4

openings. Moreover, as the variability of materials and difference in homogeneity levels for mortar and units must be considered when addressing the performance of each element type.  Thus, the use of detailed micro-models requires a relatively high level of expertise for proper application to masonry assembly behavior. Furthermore, a relatively high number of test samples are needed for experiments to capture the range of behavior for the materials i.e. units and mortar [Grecchi, 2010].

### Macro-models:

In macro-elements, none of the internal parts of the structure of the wall, i.e. units, mortar and the interface between them are modeled as separate elements. Instead, they merge together in the model to create a homogeneous anisotropic material which is used for the entire masonry assembly. Hence, the micro model mesh generated for the finite element analysis does not need to follow the pattern of bonding between units. Thus, the macro-models require significantly lower expertise levels for modeling  and a much lower computational effort is needed for  macro-models when compared to micro-models; and is therefore, much more application and design oriented. Moreover, no specific considerations need be made for modeling the openings in macro-models. In addition, as the units, mortar and the interface between them are merged to create a homogeneous anisotropic material, only the relation between average stresses and average strains in the homogenized media has to be described. Finally, a smaller number of tests on unit and mortar assemblies are needed to define the material properties for the whole infill wall assembly [Lourenço, 1996].

### Modeling preference:

Because of the following reasons, a macro-modeling approach has been selected over the micro-modeling approaches in this research:

5

1. In contrast to the micro-elements that require the separately modeling of all units and mortar layers, the macro-models can be used to divide the infill wall into geometrically appropriate wall-sections without consideration of bonding patterns and unit sizes. The wall elements can be defined regardless of the thickness of mortar layers and the location and number of units. This is useful in modeling perforated infill walls, where the openings may not necessarily follow the masonry bonding pattern.

2. Use of micro-elements requires higher levels of expertise both in masonry material behavior and Finite Element modeling when compared to macro-elements. This expertise is required especially for mesh generation, conducting frequent small size experimental tests on mortar and units to find their material properties, placing additional potential crack/slip planes to model the interface between the units and mortar and technical details to define the failure criteria of different elements.

3. Use of macro-element modeling requires much less computational effort comparing to the micro-elements. In addition, macro-elements can be calibrated with smaller numbers of experimental tests (or code defined assembly strengths and stiffness), while giving acceptably precise prediction of the overall performance of the infill walls.

In the following section a brief literature review is provided for some of the best known macro-models proposed by other researchers for modeling the in-plane behavior of infill wall systems.

## Previous Macro Models For Infill Shear Walls

Over the past sixty years, a number of researchers have investigated the behavior of infilled shear walls and frames under in-plane loading. One of the first people who proposed a model for consideration of infill shear walls was Polyakov, who suggested that the effect of an infill wall could be captured by replacing it with diagonal bracing [Polyakov 1960]. Using this idea of replacing the shear wall with a diagonal brace, many researchers proposed models where the infill wall was replaced by a single compressive strut. Each of these researchers, ([Holmes 1961], [Smith 1962, 1966], [Smith et al. 1969], [Mainstone 1971, 1974], [Bazan et al. 1980], [Liauw et al. 1984], [Paulay et al. 1992], [Durrani et al. 1994], and [Flanagan et al. 1999, 2001]) suggested different criteria for calculation of the strut width. For example, Holmes in 1961 suggested a model in which, the infill wall was replaced by a pin-joint diagonal strut made from the same material, i.e. masonry. In his model the thickness of the strut was equal to that of the wall but its width was one third of the length of the strut [Holmes 1961]. In 1962, based on the results of experimental data, Smith suggested that one third for the ratio of strut width to strut diagonal length is an overestimation; he suggested that the width of the strut to range from 0.1 to 0.25 of the length of the diagonal strut [Smith 1962]. Later in 1969, Smith et al. suggested that the width of the diagonal strut is related to the ratio of stiffness of infill wall to stiffness of frame; indeed they showed that the width of compression strut is related to the coefficient shown in Equation 1-1.

$$\lambda_h = h \sqrt[4]{\frac{E_w \, t_w \sin(2\theta)}{4 \, E_c \, I_c \, h_w}}$$    Eq. 1-1

In which, $h$ is the height of columns from centerlines of top and bottom beams, $E_w$ is the modulus of elasticity for infill wall material, $t_w$ is the thickness of the infill wall,

$E_cI_c$ is the flexural rigidity of columns, $h_w$ is the height of infill wall and $\theta$ is as following:

$$\theta = \arctan(h_w/L_w)$$  Eq. 1-2

Where, $L_w$ is the horizontal length of the infill wall and $h_w$ is the same as before.
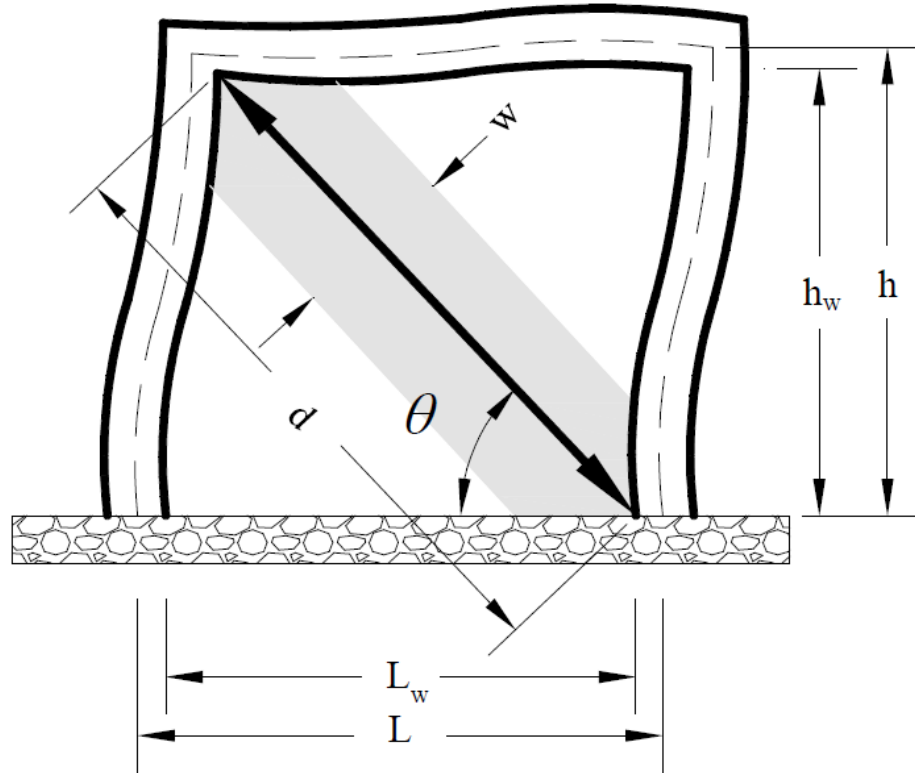


Figure 1. 2. Single Compressive Strut Model for Masonry Infill; (Fig. is based on a similar Fig. in [Asteris 2011])

In 1974, Mainstone et al. suggested a formula for the width of the equivalent compressive strut based on the relative stiffness of infill wall to stiffness of frame as following [Mainstone 1974]:

$$w/d = 0.175\,\lambda_h^{-0.4}$$  Eq. 1-3

In which, $\lambda_h$ is defined as in work of Smith et al. [1969]; see Equation 1-1. Later many other researchers ([Klingner and Bertero 1978], [Fardis and Calvi 1994], [Fardis and Panagiotakos 1997], [Kodur et al. 1995 and 1998], [Balendra et al 2003])

agreed with the Mainstone suggested formula for equivalent compressive strut width and it was also considered in FEMA 1997 [Asteris 2011].

In 1984, Tassios suggested the formula shown below (Eq. 1-4) for the equivalent compressive strut width [Tassios 1984] based on the experimental work of Bazan et al. [1980].

$$w/d = 0.2 \sin(\theta) \sqrt{(E_c A_c)/(G_w A_w)}$$ Eq. 1-4

Their proposed formula was applicable only if:

$$1 < (E_c A_c)/(G_w A_w) < 5$$ Eq. 1-5

Liauw et al. also proposed a formula for the width of the equivalent compressive strut, which was computed only for the practical strut angle, $\theta$, values of 25 and 50 for as follows [Liauw et al. 1984]:

$$w/d = (0.95 \sin\theta)/\left(2\sqrt{\lambda_h}\right)$$ Eq. 1-6

In 1987, Decanini et al. suggested two different equations for the width of the equivalent strut for cracked and uncracked infill walls [Decanini 1987]:

$$w/d = 0.01 + 0.707/\lambda_h \quad , \quad (if\ cracked\ and\ \lambda_h \leq 7.85)$$ Eq. 1-7

$$w/d = 0.04 + 0.470/\lambda_h \quad , \quad (if\ cracked\ and\ \lambda_h > 7.85)$$ Eq. 1-8

$$w/d = 0.085 + 0.748/\lambda_h \quad , \quad (if\ Uncracked\ and\ \lambda_h \leq 7.85)$$ Eq. 1-9

$$w/d = 0.130 + 0.393/\lambda_h \quad , \quad (if\ Uncracked\ and\ \lambda_h > 7.85)$$ Eq. 1-10

In 1992, Paulay and Priestley proposed a more conservative formula (Eq. 1-11) for the width of diagonal compressive struts as they showed that previous proposed criteria for width of the compressive strut may result in stiffer structure and a higher seismic load demand in the structure under lateral loading [Paulay and Priestley 1992].

$$w/d = 1/4$$ Eq. 1-11

9

All of the aforementioned formulae are based on the ratio of stiffness of infill wall to the stiffness of frame and used the ratio shown in Equation 1-1.

In 1994, Durrani et al. proposed the following formula for the width of diagonal compressive strut. It was also based on the relative stiffness of infill wall and frame but it did not use the $\lambda_h$ calculated by Equation 1-1 [Durrani et al. 1994].

$$w/d = \gamma \sin(2\theta) \qquad\qquad \text{Eq. 1-12}$$

Where,

$$\gamma = 0.32 \sqrt{\sin(2\theta)} \left( \left(h^4 E_w t_w\right) / \left(m E_c I_c h_w\right)\right)^{-0.1} \qquad\qquad \text{Eq. 1-13}$$

In which,

$$m = 6\left(1 + \left(6 E_b I_b h\right) / \left(\pi E_c I_c L\right)\right) \qquad\qquad \text{Eq. 1-14}$$

And, $E$, $I$ and $h$ are abbreviations for elasticity modulus, the moment of inertia and the height, while the subscripts $w$, $c$ and $b$ denote wall, column and beam, respectively.

However, many researchers found that the single compressive strut model could not reproduce the flexural moments and shear forces created in the frame members and showed that diagonal strut models did not accurately address all aspects of the interaction between the frame and the infill; ([Reflak et al. 1991], [Buonopane et al. 1999], [Chaker et al. 1999], [Mohebkhah et al. 2007] and [Asteris et al. 2011] among many others). In addition, there were still disagreements about the width of equivalent strut considered in the modeling process. Furthermore, single-strut models usually underestimated the flexural capacity of the wall as the lateral forces were primarily resisted by a truss mechanism [Crisafulli 1997].

In 1995, Saneinejad proposed a method for the analysis and design of infilled steel frames under in-plane loading, which was later used by [Madan et al. 1997]. Saneinejad used nonlinear finite-element analyses calibrated on previous experiments and assumed that wall openings were not along the formed diagonal struts. A number

10

of researchers applied the strut model to perforated infill walls and found that the lateral resistance, initial stiffness and energy dissipation capacity of perforated infill walls could be significantly lower than solid infill walls ([Benjamin et al. 1958], [Mallick et al. 1971], [Liauw et al. 1977], [Utku 1980], [Giannakas et al. 1987], [Al-Chaar et al. 2003], [Asteris 2003], [Mohebkhah et al. 2007] and [Mondal et al. 2008]). However, modifications of the model to account for openings typically just reduced the width of single compressive strut [Kakavetsis et al. 2009] and can become very inaccurate for modeling the infill walls with openings.

In 1976, Leuchars and Scrivener [1976] proposed a model for masonry infill shear walls that considered sliding shear failure; the model had two struts and was able to predict large the bending moments and shear forces that are often induced in the central zone of the frame columns. The wall sliding friction mechanism (along cracks) was also considered by the model using an element connecting the two struts. To model the interaction between frame and infill more precisely, [Thiruvengadam 1985] proposed the use of a multiple strut model for infill walls. His model was originally intended to more realistically evaluate the natural frequencies and vibration modes of infill shear walls.

Other researchers, also proposed multiple strut models, [Syrmakezis et al. 1986], [Chrysostomou 1991], [Chrysostomou et al. 2002]. [Syrmakezis et al. 1986] suggested the use of five parallel diagonal struts, in both directions, to emphasize on the effect of frame-infill contact length on distribution of moments in the surrounding frame.

Chrysostomou focused on the degradation of stiffness and strength of the infill shear walls, and suggested the use of six compression-only diagonal struts, in both directions [Chrysostomou 1991]. In this model, the ends of off-diagonal compression-

11

only struts were inserted on the potential plastic hinge locations on the beams and columns and only half of the six struts were active under loading in each direction.
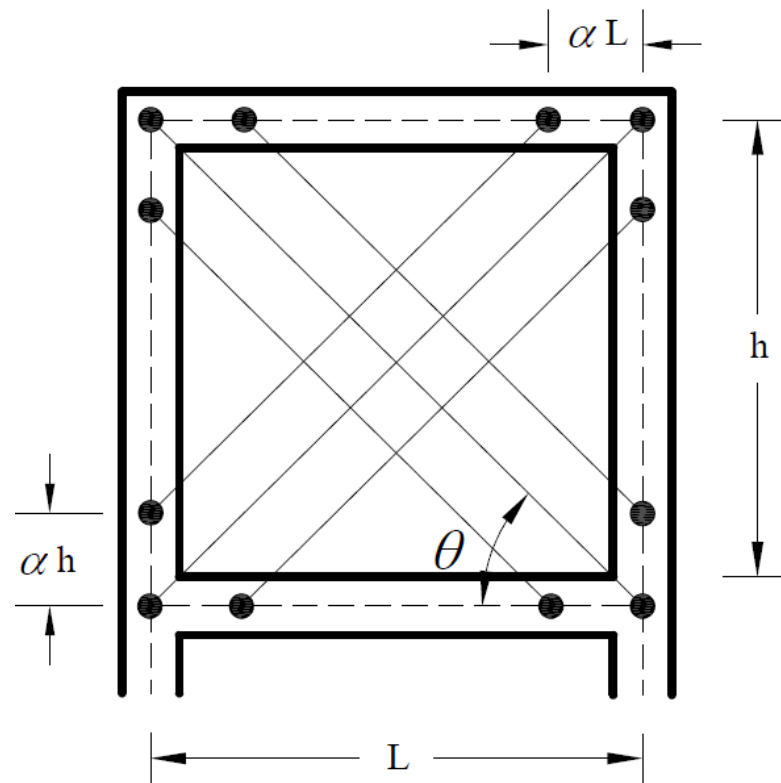


Figure 1. 3. Parallel Multiple-Struts Model for Masonry Infill Walls [Chrysostomou 1991];(Fig. is based on a similar Fig. in [Asteris 2011])\

[El-Dakhakhni et al. 2001], [El-Dakhakhni 2002] also suggested a model that used one diagonal and two off-diagonal struts in order to describe the orthotropic behavior of the masonry. This model was later adopted by [Mohebkhah et al. 2007] to consider the nonlinear global behavior of infilled steel frames with central openings.
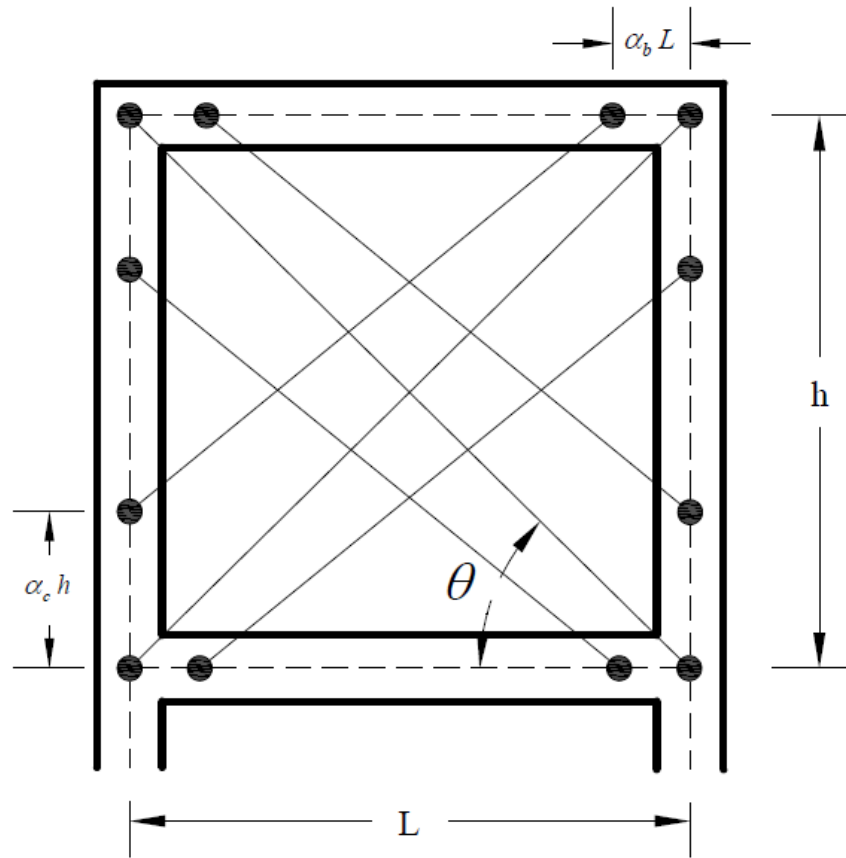
Figure 1. 4. Non-Parallel Multiple-Struts Model [El-Dakhakhni et al. 2001]; (Fig. is based on a similar fig. in [Asteris 2011])

In his Ph.D. thesis, Crisafulli showed that even the most complicated multiple-strut model, such as that proposed by Thiruvengadam [1985] was not capable of describing the response of the infilled frame systems when horizontal shear sliding occurs in the masonry panel [Crisafulli 1997]. Thus, he modified the model of Leuchars and Scrivener by implementing a four-node panel element connected to the frame at the beam-column joints [Crisafulli et al. 2007]. Although the modified model was easy to use in the analysis of infilled frame structures, it did not accurately predict the bending moments and shear forces in the surrounding frame [Asteris et al. 2011].
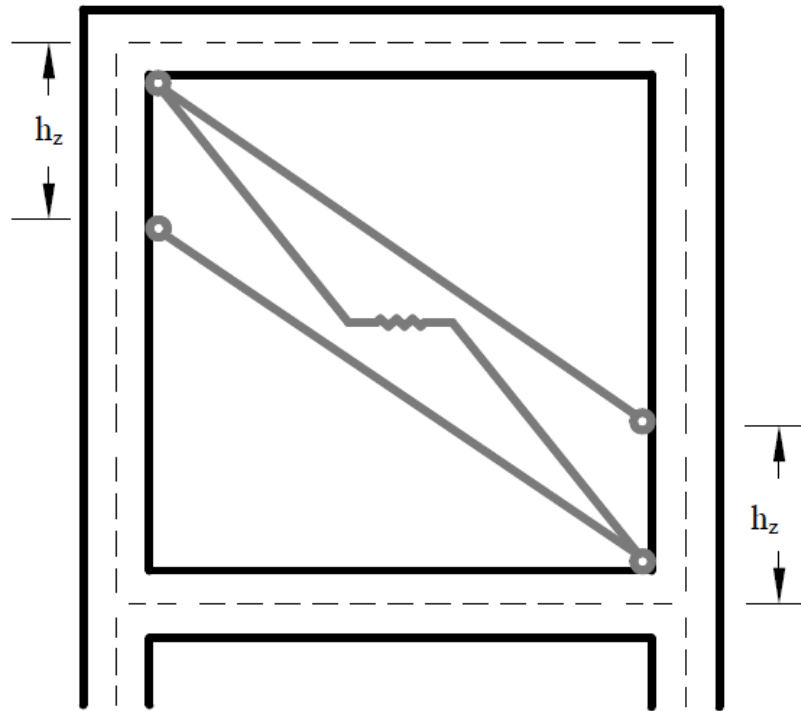
Figure 1. 5. Multiple-Strut Model for Masonry Infill Walls [Crisafulli et al. 2007];
(Fig. is based on a similar Fig. in [Asteris 2011])

Finally, in all of these models, the force-displacement relationships of the equivalent-strut model must account for the nonlinear hysteretic material behavior, which increases the computational complexity and uncertainty of the problem [Asteris et al. 2011].

In conclusion, neither the single strut models nor the multi-strut models were accurate enough to predict the performance of masonry infill shear wall systems. Previous models lack the ability to consider all types of common failure modes and most of them cannot properly address the effects of wall openings. In addition, modeling steel reinforcement has not been properly addressed in the previous models. As a result, there is a need for an analytical model that is able to predict the behavior of these structural systems, more accurately.

Recently, a new macro-element was proposed by Caliò et al. [2012] to assess the performance of masonry structures under lateral and vertical loadings. Caliò et al.

later used their model for masonry structures in studying the behavior of infill walls [Caliò et al. 2014]; see Fig. 1-5.
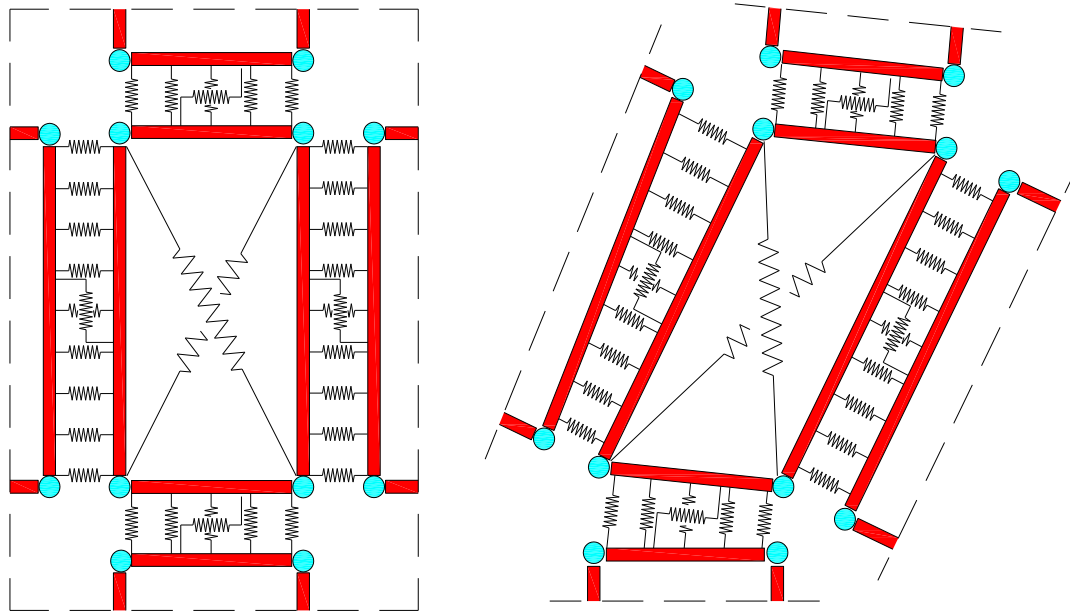


Figure 1. 6. Macro-Element Proposed by [Caliò et al. 2012]

(a) Undeformed Configuration (b) Deformed Configuration (reprinted from [Caliò et al. 2012] with permission)

**Proposed Macro Model for Infill Masonry Shear Walls**

In the current research, the model proposed by [Caliò et al. 2012] was modified and extended to capture the shear deformations of the masonry shear walls more accurately. In addition, the effect of doweling action of reinforcement on the shear transfer mechanisms was also considered by the proposed model. Moreover, the model's description of the impact of steel reinforcements on the shear and in flexural behavior of the shear walls was enhanced in this research. Finally, the frame-infill contact problem has also been addressed using the multiple constraint contact problem procedures   and the Lagrange Multipliers method. A detailed description of

www.manaraa.com

the macro-element developed in this by this investigation will be presented in the following Chapter.

# CHAPTER 2 : MODEL DEVELOPMENT

To address some of the shortcomings of the previously described models, a new macro-element for modeling both reinforced and unreinforced masonry infill shear walls is proposed and its development is described in this chapter. In the first section, the model for unreinforced masonry infill shear walls will be described. Following sections present how the model will account for the effects of steel reinforcement on the different behaviors of masonry infill shear walls and an element for capturing the frame-infill shear wall and frame interaction and possible methods for applying the contact to the finite element equations.

The macro element presented in this chapter is based on an element previously developed by Ivo Caliò et al. who proposed a new modeling approach and developed an analysis program for the simulation of seismic behavior of masonry structures [Caliò et al. 2012]. In his modeling approach, Caliò developed a rigid bar macro element that used a series of springs to capture the flexural behavior of infill wall. In addition, Calio's model used a set of two diagonal springs to model the shear behavior of the shear wall elements. Finally, a nonlinear rigid-plastic link addressed the shear transferred between any two wall sections. Caliò et al. showed that their element gave reasonably accurate predictions of the behavior of solid masonry walls and infilled frames with relatively low computational effort. The element proposed in this chapter extends the macro element developed by Caliò et al. to produce a more accurate prediction of the behavior of infill shear walls fully or partially confined within a

17

frame. Moreover, the problem of contact between frame and infill wall is addressed using a new "gap" element.

Indeed, in the proposed model, gap elements are used to account for any compressive contact between the frame and the infill wall. The gap elements, if closed, capture the frame-infill shear wall contact effects, and then they can be applied to the finite element equations using the Method of Lagrange Multipliers. It is worth mentioning that the values computed for the Lagrange Multipliers are equal to the forces transferred to/from frame from/to infill wall; thus they can be used to locally study the frame-infill contact problem in more detail.

As shown in Fig. 2-1, the proposed macro element is configured to model flexural and shear deformations. Also, the shear transferred between any two contiguous elements can be captured using a set of nonlinear links that connect them along their common interface. Variable meshing of these elements will produce the desired precision and account for openings, if present. It should be noted that this model only describes the in-plane behavior of infill walls, and the work presented herein is limited to single story one bay frames. However, it is expected that larger structural systems can be readily analyzed using this modeling system.

As shown in Figure 2-1, the proposed macro-element consists of four rigid bars, hinged at their ends, forming a rectangular chassis to which three different groups of springs are attached. The rigid bars are stabilized using ten linear/nonlinear "shear" springs that are used to describe the shear behavior of the infill wall. In addition, there are groups of linear/nonlinear zero-length springs attached perpendicularly to the rigid bars of adjacent elements, simulating the flexural behavior of the infill shear wall. Finally, a pair of rigid-plastic links connecting the parallel rigid bars along adjacent

18

element edges are simulating the shear transfer mechanism between macro-elements and capturing any sliding shear failure. The constitutive relations for each group of springs, along with their calibration procedures are described later in this work and are based on simple behavior models and masonry code derived capacities.
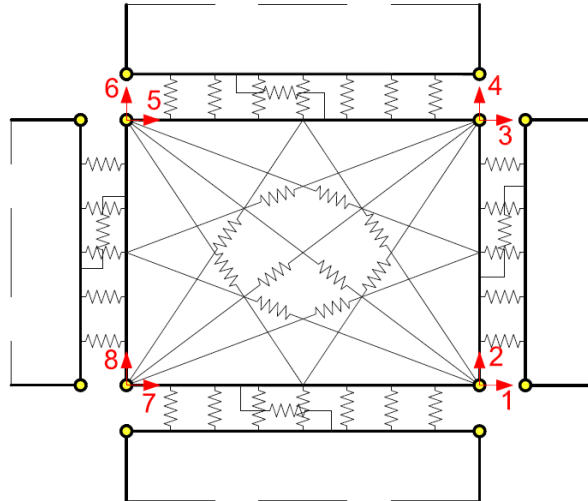


(a). Undeformed Shape of Proposed Macro-Element
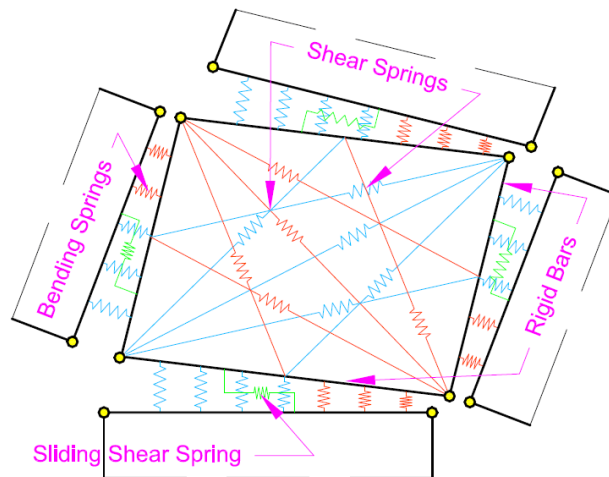


(b). Deformed Shape of Proposed Macro-Element
Figure 2. 1. Proposed Macro-element; (Fig. is Based on a Similar Fig. in [Caliò et al. 2012])

To evaluate the model more clearly, Figure 2-2 separately shows the three deformations (flexural, shear and sliding shear) modeled by the proposed shear wall element.  It should be noted that an infill wall under lateral loading may exhibit one or more modes/mechanisms of failure associated with each of these deformations. The

19

proposed macro-element/model can be distinguished from previous models as described in the following:

1. The interaction of the shear wall and the frame is addressed with special contact elements (gap elements), at the joints of the rigid bars (they enable the model to capture any frame-wall compressive contact even when there are initial gaps on top or sides of the wall that may be intentional or produced by imperfect construction). These gaps lead to lower initial stiffness for the wall frame system at lower loads and will affect the frame only when closed under loading. These effects must be considered in the analysis in order to accurately predict the behavior of the structural system.

2. The additional diagonal shear springs allow the shear stiffness of the masonry infill shear wall to degrade in a more realistic manner; in the proposed model, the wall can degrade in up to three stages for the case of unreinforced infill walls and up to four stages for the case of reinforced infill walls.

3. The flexural springs allow the stiffness of the wall element to gradually degrade in a more realistic manner than the compression strut models and can be used to account for the presence of reinforcement,

4. The sliding shear nonlinear links consider the doweling action in the sliding shear transfer mechanism (if reinforcement is present) and thus capture the behavior of reinforced infill walls more realistically.

5. The constituent material models are based on masonry code mandated material properties and assembly capacities (and these are based on extensive testing) [MSJC, 2013].
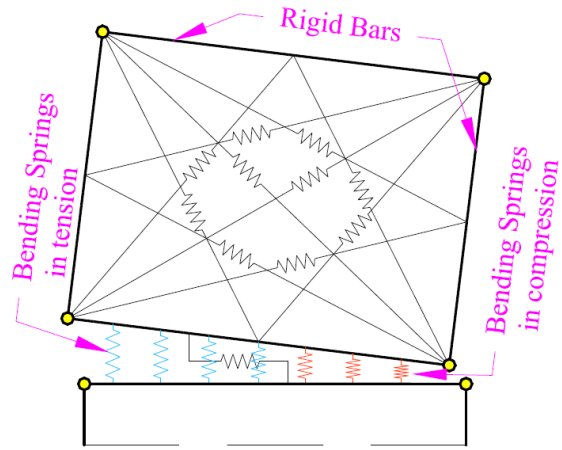
(a) Flexural Behavior
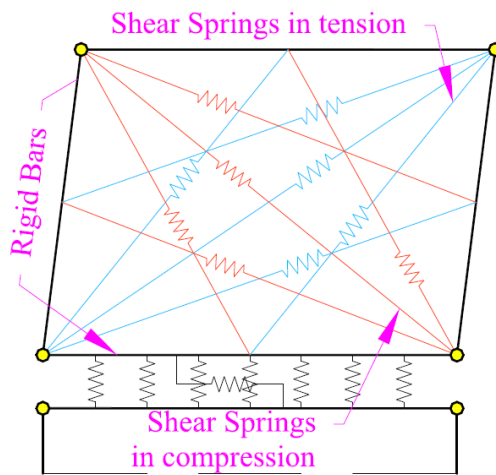


(b) Shear Behavior
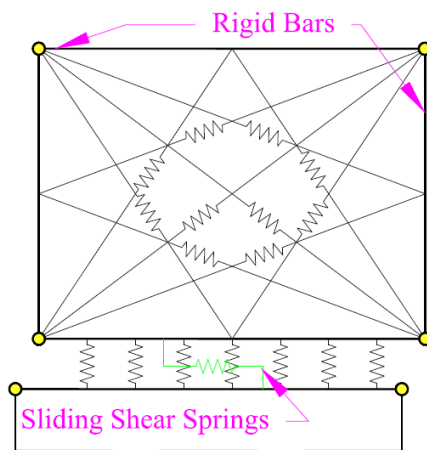


(c) Sliding Behavior

Figure 2. 2. Deformation Mechanisms/Failures of the Proposed Macro-Element (Fig. is Based on a Similar Fig. in [Caliò et al. 2012])

## Steel Reinforcement Model

### Reinforcement Participation in Flexure

Steel reinforcing bars are often used in masonry construction. These bars can participate in infill shear wall behaviors including flexural, shear and shear transfer. In flexure, the reinforcement is modeled by using additional flexural spring elements, similar to the masonry flexural spring elements. As shown in Figure 2-3, these steel springs are placed along the rigid bars of the shear wall element, at the actual location of the reinforcing.
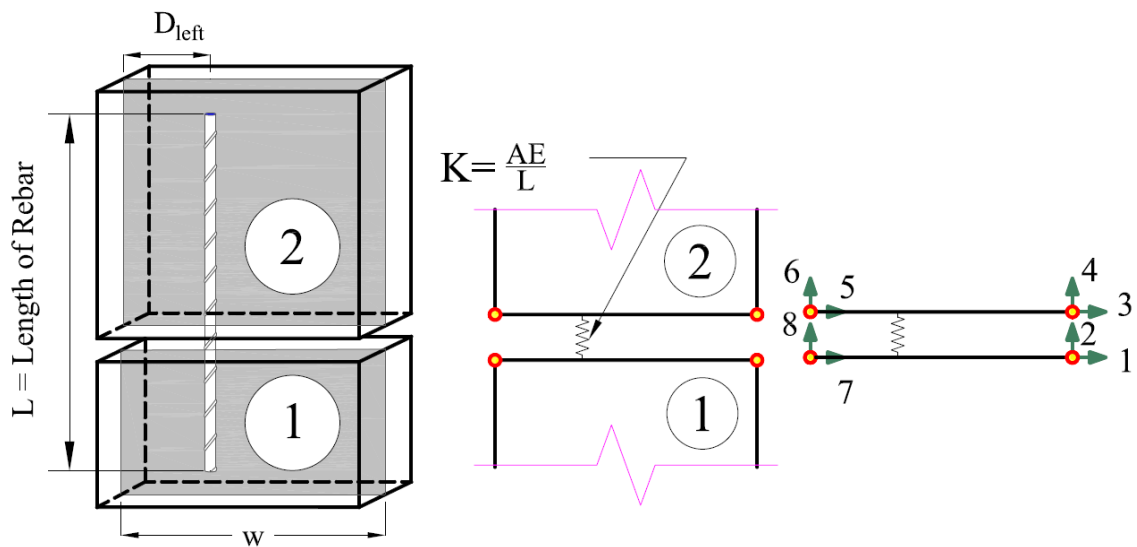


Figure 2. 3. Modeling Flexural Steel Reinforcement

### Reinforcement Participation in Shear

If high shear demand applications, steel reinforcing bars are placed in masonry shear walls to improve shear strength and ductility. The effect these reinforcements have on the strength and stiffness of the shear wall element are accounted for by equivalent truss elements. These elements shown in Figure 2-4 are used to account for any steel reinforcing bars that obliquely cross a give shear wall macro-element.

22
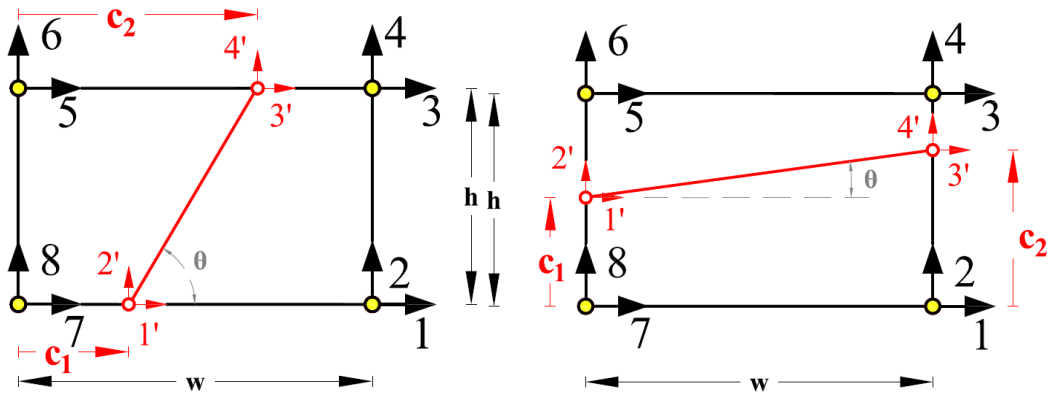
Figure 2. 4. Modeling of Steel Shear Reinforcement

**Frame-Wall Contact**

As the infill walls are usually constructed after the surrounding frame has finished, the distance between them cannot be properly filled with grouting; thus, there is usually a gap between the frame and the shear wall even it was not intended. As the frame deforms it will close the gap at some points and place the frame in contact with the shear wall.  As these contact points are the only ways of transferring load between the wall and the surrounding frame, the load distribution between frame and shear wall can significantly change depending on the size of the gaps and locations of the contact points. The occurrence and location of contact depends on wall and frame deformations and the size of the gap.

Assume an infilled frame with the gaps on top and sides of the wall, as shown in Fig. 2-5.
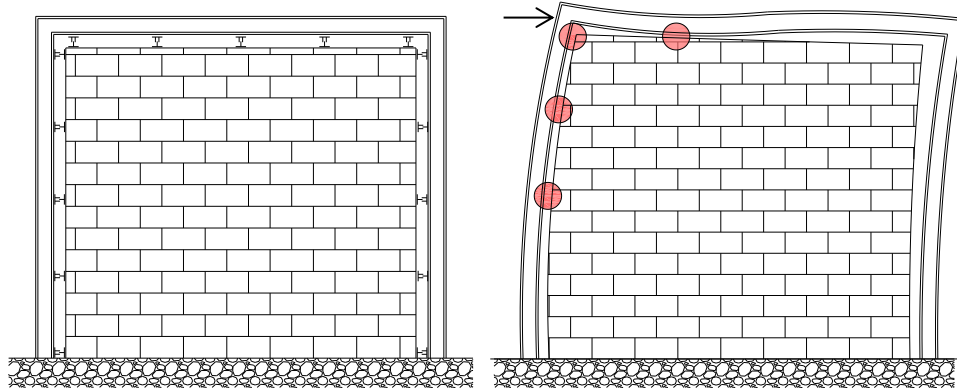
(a) Gap Elements between Frame and Infill Wall            (b) Points of Contact

Figure 2. 5. Finding the Points of Contact Between the Infill Shear Wall and Frame
Using Gap Elements

The gap elements shown in Fig. 2-5-a. are inserted in order to monitor the relative displacements of frame and infill wall at predefined locations. Each gap element has two confronting parts which are connected to the wall and frame. As the frame and infill wall cannot pass through each other when the gap element is closed under loading, additional constraints will be added to the finite element equations to ensure this is accounted for. This constraint process is known as multi-freedom constraint. In general, three methods are commonly used to apply this type of constraint to the finite element equations. These are the Penalty method, the Master-Slave method, and the Lagrange Multipliers method. The Penalty method induces approximations to the solution, while, the Master-Slave and Lagrange Multipliers methods give accurate results in linear and in linear/nonlinear zones, respectively. For the proposed model, the Lagrange Multipliers method was chosen as it gives accurate solutions in both linear and nonlinear zones. In the following discussion, the Lagrange Multipliers method is briefly described using a simple example for a homogeneous multi-freedom constraint; more information about these methods can be found elsewhere ([Park et al., 2000], and [Felippa, 2014]).

24

Consider the axially loaded bar shown in Fig. 2-6-a. (Similar to the example in work of [Felippa et al., 2014]).
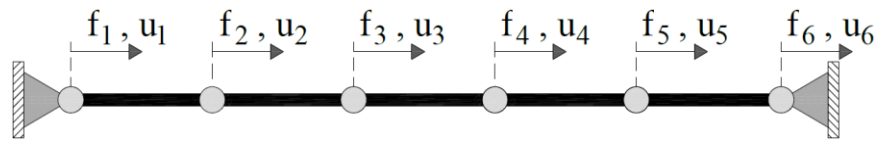


(a) Structural Example
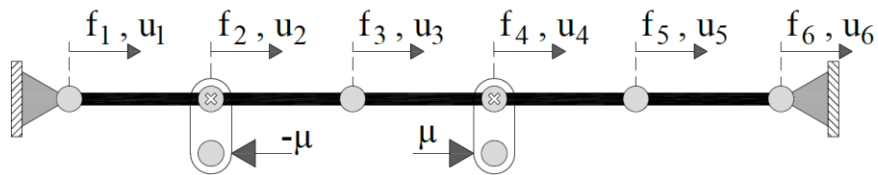


(b) Lagrange Multiplier $\mu$ (Multi-freedom Constraint)

Figure 2. 6. Structural Example for Homogeneous Multi-Freedom Constraint ( ); (modified from [Felippa, 2014], with permission)

The finite element equations for the structure shown in Fig. 2-6-a can be written as shown in Equation 2-1.

$$\begin{bmatrix} K_{11} & K_{12} & 0 & 0 & 0 & 0 \\ K_{21} & K_{22} & K_{23} & 0 & 0 & 0 \\ 0 & K_{32} & K_{33} & K_{34} & 0 & 0 \\ 0 & 0 & K_{43} & K_{44} & K_{45} & 0 \\ 0 & 0 & 0 & K_{54} & K_{55} & K_{56} \\ 0 & 0 & 0 & 0 & K_{65} & K_{66} \end{bmatrix} \begin{Bmatrix} u_1 \\ u_2 \\ u_3 \\ u_4 \\ u_5 \\ u_6 \end{Bmatrix} = \begin{Bmatrix} f_1 \\ f_2 \\ f_3 \\ f_4 \\ f_5 \\ f_6 \end{Bmatrix} \qquad \text{Eqn. (2-1)}$$

Now, assume that the multi-freedom constraint of Equation 2-2 is to be applied in addition to the constraints provided by supports, as shown in Fig. 2-6-a.

$$U_2 - U_4 = 0 \qquad \text{Eqn. (2-2)}$$

This is called a homogeneous multi-freedom constraint, as the value on the right side of Equation 2-2 is equal to zero. Physically, this multi-freedom constraint is similar to the case where a rigid bar is connected to degrees of freedom 2 and 4. If the rigid bar

25

method was used, its large stiffness would have caused singularities in the solution leading to inaccurate results. Thus, instead of adding the rigid bar, its unknown internal force can be added to the equations as shown in Equation (2-3).

$$\begin{bmatrix} K_{11} & K_{12} & 0 & 0 & 0 & 0 \\ K_{21} & K_{22} & K_{23} & 0 & 0 & 0 \\ 0 & K_{32} & K_{33} & K_{34} & 0 & 0 \\ 0 & 0 & K_{43} & K_{44} & K_{45} & 0 \\ 0 & 0 & 0 & K_{54} & K_{55} & K_{56} \\ 0 & 0 & 0 & 0 & K_{65} & K_{66} \end{bmatrix} \begin{Bmatrix} u_1 \\ u_2 \\ u_3 \\ u_4 \\ u_5 \\ u_6 \end{Bmatrix} = \begin{Bmatrix} f_1 \\ f_2 - \mu \\ f_3 \\ f_4 + \mu \\ f_5 \\ f_6 \end{Bmatrix} \qquad \text{Eqn. (2-3)}$$

The $\mu$ is called a Lagrange Multiplier and its value is unknown; by transferring it to the vector of unknowns we will have:

$$\begin{bmatrix} K_{11} & K_{12} & 0 & 0 & 0 & 0 & 0 \\ K_{21} & K_{22} & K_{23} & 0 & 0 & 0 & +1 \\ 0 & K_{32} & K_{33} & K_{34} & 0 & 0 & 0 \\ 0 & 0 & K_{43} & K_{44} & k_{45} & 0 & -1 \\ 0 & 0 & 0 & K_{54} & K_{55} & K_{56} & 0 \\ 0 & 0 & 0 & 0 & K_{65} & K_{66} & 0 \\ 0 & +1 & 0 & -1 & 0 & 0 & 0 \end{bmatrix} \begin{Bmatrix} u_1 \\ u_2 \\ u_3 \\ u_4 \\ u_5 \\ u_6 \\ \mu \end{Bmatrix} = \begin{Bmatrix} f_1 \\ f_2 \\ f_3 \\ f_4 \\ f_5 \\ f_6 \\ 0 \end{Bmatrix} \qquad \text{Eqn. (2-4)}$$

After applying the constraints due to the supports of the structure and solving the system of equations written in Equation 2-4, the displacements and the Lagrange multiplier $\mu$ can be computed. Note that, the value calculated for $\mu$ is equal to the force created in the rigid bar if it was physically added to the system. This was a homogeneous multi-freedom constraint applied by using the Lagrange Multipliers method. Similarly, multiple homogeneous multi-freedom constraints can be added. Information about the nonhomogeneous multi-freedom constraints can be found in work of [Felippa, 2014].

In the proposed infill shear wall model, closure of a gap element is defined by a negative distance between its confronting parts. Thus, even when the distance between parts of gap element are zero it is not considered closed as the sides are not pushing toward each other. This definition allows us to model the contact problem when there is not an initial gap between the infill wall and surrounding frame.

In places where the frame and infill wall are in contact under compression, the gap elements are defined as closed and multi-freedom constraints are derived, correspondingly. As the deformations of nonlinear springs of the proposed macro elements are based on the displacements of corners of the rigid bars (chasses), the gap elements are placed between frame and macro elements only at the corners of the macro element chasses; see Fig. 2-7-b.
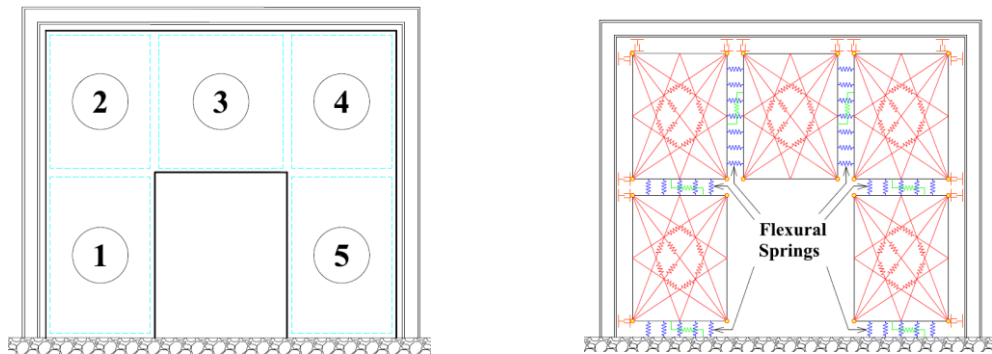


(a) Infill Wall with Door Opening      (b) Flexural Springs and Gap Elements

Figure 2. 7. Steel Frame with Perforated Infill Wall (Door Opening)

# CHAPTER 3 : MODEL ELEMENT AND BEHAVIOR CALIBRATION

In this chapter, the procedures used to define the response of all three types of springs of the proposed macro model, along with the springs proposed to represent the different effects of reinforcements (if present) are presented. In the first section, the required procedures used to define the unreinforced masonry infill shear walls will be presented. Later, the procedures for modeling the reinforcements both in shear and flexure are presented.

## Unreinforced Masonry Infill Shear Walls

In case of unreinforced masonry infill walls, the response of the flexural springs, shear springs and sliding springs are based on theoretical and/or experimental data. In the following sections, the response of each of these spring types will be described along with the procedures used to calibrate each spring model.

## Linear/Nonlinear Flexural Springs

Consider a masonry infill wall with door openings as shown in Fig. 3-1-a (duplicated from Chapter 2 for convenience). This wall can be divided into five sections as shown with dashed lines in figure and each section defines a macro element (see Figure 3-1-b. All of the macro-elements are connected to their adjacent macro-elements with sets of flexural tension-compression springs at right angles to rigid bars in each macro element. These springs, shown in Fig. 3-1-b, are intended to simulate the flexural resistance of the wall using a fiber-modeling approach.

28
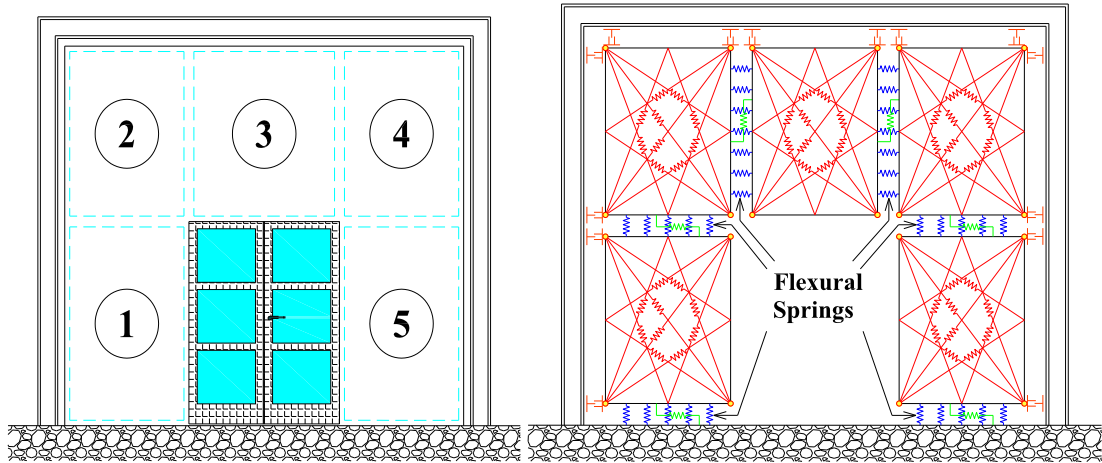
(a) Infill wall with door opening    (b) Flexural Springs in the Macro-model

Figure 3. 1. Infilled Steel Frame with Door Opening

(Figure duplicated from Chapter 2 for convenience).

As shown in Figure 3-2, there are flexural springs connecting the rigid bars of two adjacent macro-elements, thus placing each pair of flexural springs in series. While in the computational model these springs have zero length, the stiffness of the flexural springs is calculated based on the assumption that they are extended to the center-lines of contiguous macro-elements. The effective stiffness of each of the springs in series is calculated using Equation (3-1) and the resultant stiffness for a spring equivalent to each pair of springs in series (shown in Fig. 3-2-c) can be determined using Equation (3-2).
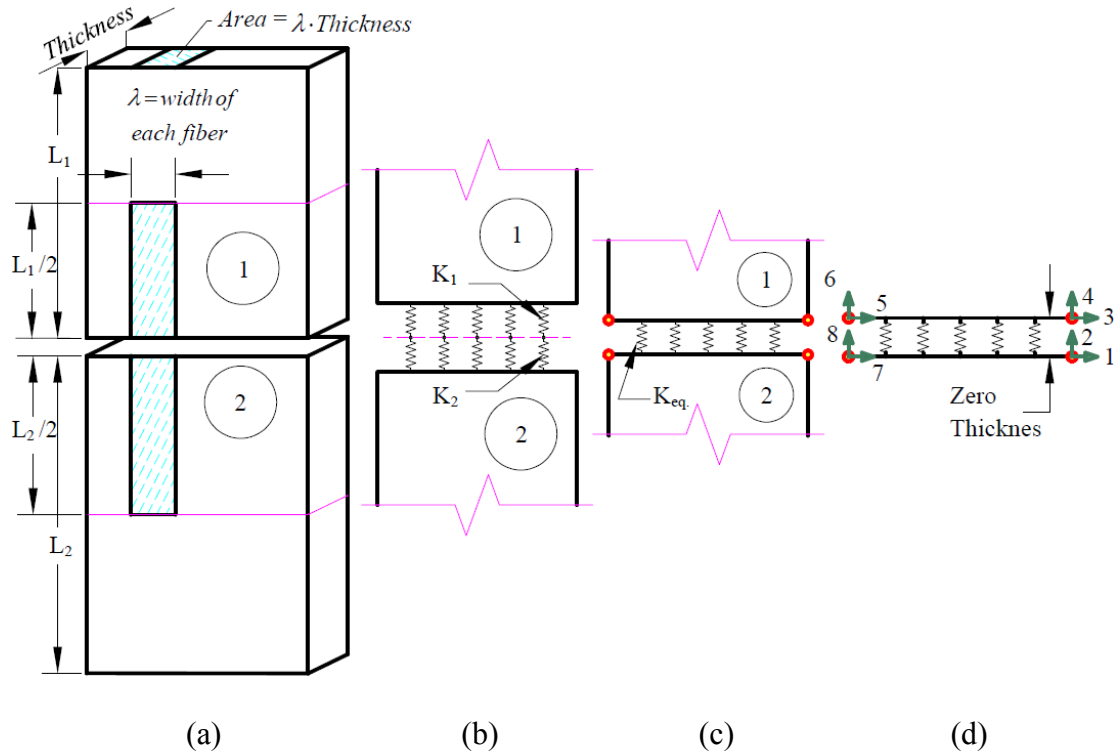
Figure 3. 2. Flexural Springs Stiffness Formulation

a) Two Adjacent Wall-Parts, b) Springs Defined by Each Wall Part, c) Set of Equivalent Springs, d) Flexural Element using Variable Number of Zero-Length Springs in the Interface with Defined Degrees of Freedom (Fig. is Based on a Similar Fig. in [Caliò et al. 2012]).

$$k_i = \frac{E_i \cdot \lambda \cdot t}{(L_i/2)} \qquad (i = 1, 2) \qquad \text{Eq. (3-1)}$$

Where, $\lambda$ equals the width of the fibers along the element and equals the interface length divided by the number of flexural springs along the interface, $L_i$ is the length of each element perpendicular to the interface and $t$ is the thickness of the infill wall.

$$K_{eq} = \frac{k_1 k_2}{k_1 + k_2} \qquad \text{Eq. (3-2)}$$

The stiffness of the flexural element can be assembled using Equation (3-3) and the stiffness of each of the equivalent springs in series. The flexural response of each macro element includes the two connected parallel rigid bars on each face and the

flexural tensile/compressive springs in series. The deformation of each spring set is related to the corresponding degrees of freedom shown in Fig. 3-2-d.

$$K_{Flexural\,Element} = \begin{bmatrix} 0 & 0 & 0 & 0 & 0 & 0 & 0 & 0 \\ 0 & \alpha & 0 & -\alpha & 0 & -\beta & 0 & \beta \\ 0 & 0 & 0 & 0 & 0 & 0 & 0 & 0 \\ 0 & -\alpha & 0 & \alpha & 0 & \beta & 0 & -\beta \\ 0 & 0 & 0 & 0 & 0 & 0 & 0 & 0 \\ 0 & -\beta & 0 & \beta & 0 & \alpha & 0 & -\alpha \\ 0 & 0 & 0 & 0 & 0 & 0 & 0 & 0 \\ 0 & \beta & 0 & -\beta & 0 & -\alpha & 0 & \alpha \end{bmatrix}$$
Eq. (3-3)

Where $\alpha$ and $\beta$ are defined as following.

$$\alpha = \frac{\lambda \cdot t}{(L_1 + L_2)/2} \left[ \sum_{i=0}^{n-1} \left( \frac{2i+1}{2n} \right)^2 E_{i+1} \right]$$
Eq. (3-4)

$$\beta = \frac{\lambda \cdot t}{(L_1 + L_2)/2} \left[ \sum_{i=0}^{n-1} \left( \frac{2i+1}{2n} \right) E_{i+1} \right] - \alpha$$
Eq. (3-5)

$\lambda$ is the fiber width associated with each spring, $t$ is the thickness of the wall and $L_i, i = 1, 2$ are the perpendicular lengths of the adjacent panels connected at the interface. $n$ is the number of springs. $E_i$ is the elasticity modulus of the ith fiber.

This approach is quite simple and if a sufficient number of springs are used to define each macro element, it produces a reasonable estimate of the flexural performance of the masonry infill shear wall segment. A more advanced modeling approach could be used, if pairs of springs in series are separately used to determine $\alpha$ and $\beta$ values. If the latter approach had been chosen, the failure criterion could have been checked for each spring [Caliò et al. 2012].

The relative corner displacements of adjacent elements' rigid bars are used to determine the strain for each flexural spring under applied loadings. This allows each

31

spring pair to soften separately as defined by the masonry material model. In the modeling, each spring is initially assigned equal elasticity moduli in tension and compression. If a spring fails in tension, then spring stiffness is softened (tensile elastic modulus is lowered) according to the constitutive relation but the compression stiffness (compressive elasticity modulus) will remain unchanged. Thus, if a spring fails in tension it can still provide resistance in compression. On the other hand, if a spring fails in compression, the compression stiffness is softened (compressive elastic modulus is lowered) according to the constitutive relation and the tensile stiffness (elasticity modulus) will be assumed to drop to near zero. It is reasoned that masonry that has substantially degraded due to high compressive strains will have little tensile resistance. Thus, the modeling techniques are capable of capturing pinching effects observed under cyclic loading.

**Linear/Nonlinear Shear springs:**

Each macro-element contains ten internal springs connected to the corners and midpoints of the rigid bar chassis on the element edges. These ten springs can be collected in three groups, corner-to-mid-height (Type-1), corner-to-mid-width (Type-2) and corner-to-corner springs (Type-3); see Fig. 3-3-a and 3-3-b. Fig. 3-3-c shows the angle each group of springs makes with the including rigid bars.

(a) Single wall    (b) Proposed Macro Model with Shear Springs    (c) Spring Angles
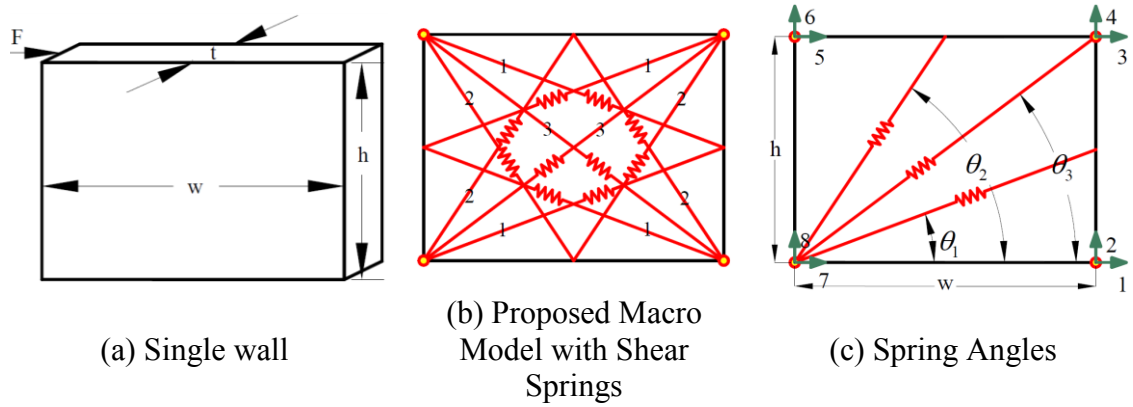
Figure 3. 3. Wall Macro Model Shear Elements (Springs)

Type 1 (4 Springs); Type 2 (4 Springs); Type 3 (2 Springs);

In order to determine the stiffness of each of the shear springs, the shear stiffness of the shear wall element was determined using the classic horizontal shear stiffness formula shown by Equation (3-6).

$$K = (G. A_t) / h \qquad \text{Eq. (3-6)}$$

Where, $G$ is the modulus of rigidity, $A_t$ is the shear area defined by the wall width times its thickness and $H$ is the wall height.

Consider an angular deformation, $\gamma$, for the chassis of macro-element; this can cause a horizontal or vertical displacement as shown in Figs. 3-4-a and 3-4-b, respectively. Now, consider the two Type 1 shear springs shown in Fig. 3-4. The projected elongation of each of these springs in x-direction, equals $\delta_h/2$, while the horizontal displacement of top of the macro-element equals the sum of projected elongations of each of the springs, i.e. ($\delta_h = \delta_h/2 + \delta_h/2$). Thus, the two Type 1 springs will act as springs in series, horizontally (Fig. 3-4-a). On the other hand, the projected elongation of each of these springs in the y-direction, equals $\delta_v$, which equals the vertical displacement of right side of the element, i.e. $\delta_v$ (Fig. 3-4-b). Hence, the Type 1 springs will act as parallel springs, vertically.
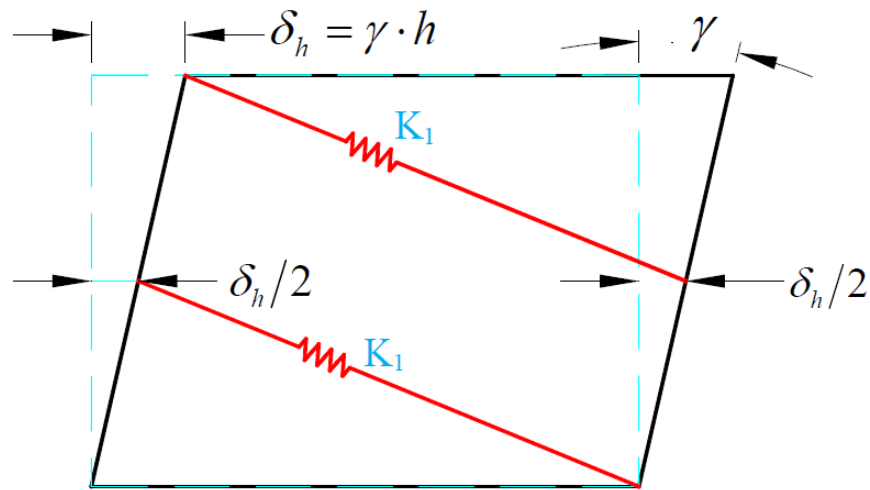
(a) $K_1$ Springs, in Series (horizontally)
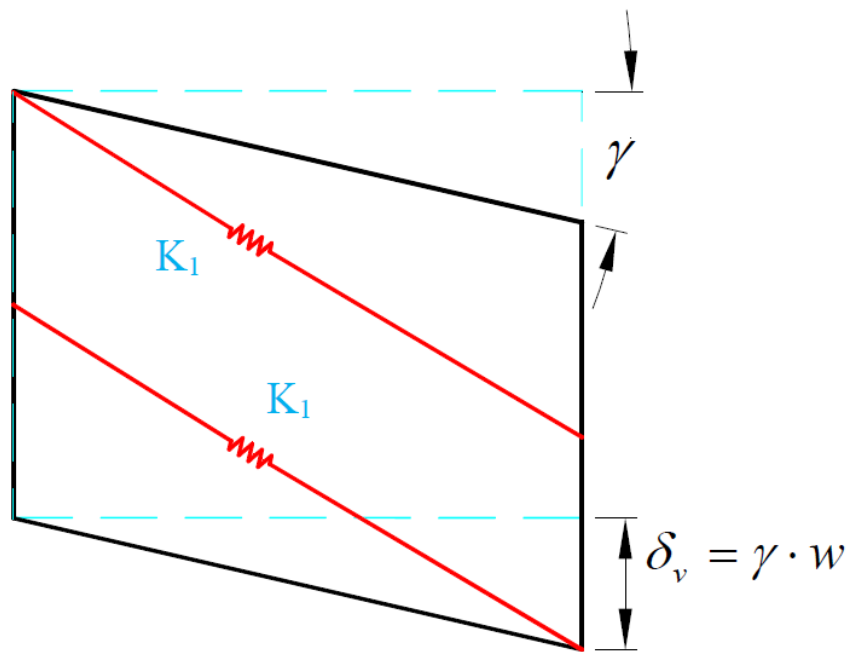


(b) $K_1$ Springs, in Parallel (Vertically)

Figure 3. 4. Type 1 Shear Springs in x and y Directions

Note that, as one end of spring Types 1 and 2 are connected to the middle point of a rigid bar, the deformation of each of these springs can be only calculated based on displacements of three corners of the macro-element. Hence, the stiffness of spring Types 1 and 2 cannot directly be compiled into the macro-element stiffness matrix.

www.manaraa.com

Instead, the shear stiffness of the macro-element must be derived by simultaneously summing up the effective resistance of all ten springs.

Each Type-1 spring has an anisotropic contribution to the shear stiffness of the macro-element, where the stiffness of each Type-1 spring in the x and y directions equals $K_1/2$ and $K_1$, respectively. Thus, to model such behavior, a non-orthogonal transformation matrix must be utilized to map the stiffness of each Type 1 spring from the local coordinate system to the macro-element coordinate system. The non-orthogonal transformation matrix for Type 1 shear springs is shown in Equation 3-7.

$$T_1 = \begin{bmatrix} C/\sqrt{2} & -S \cdot \sqrt{2} & 0 & 0 \\ S \cdot \sqrt{2} & C/\sqrt{2} & 0 & 0 \\ 0 & 0 & C/\sqrt{2} & -S \cdot \sqrt{2} \\ 0 & 0 & S \cdot \sqrt{2} & C/\sqrt{2} \end{bmatrix}$$

Eq. (3-7)

In which,

$$C = \cos(\theta_1), \quad S = \sin(\theta_1) \text{ and } \theta_1 = \arctan(h/2w)$$

Eq. (3-8)

In contrast, for the two Type-2 springs shown in Fig. 3-5, projection of each spring's elongation in the x-direction equals $\delta_h$, which is equal to the horizontal displacement of top of macro-element; thus, the Type 2 springs act as parallel springs, horizontally. However, the sum of projections of each of the type two spring's elongation in y-direction equals the vertical displacement of right side of macro-element i.e. ($\delta_v = \delta_v$ /2+ $\delta_v$ /2); thus, the two Type 2 springs are in series, vertically.

35
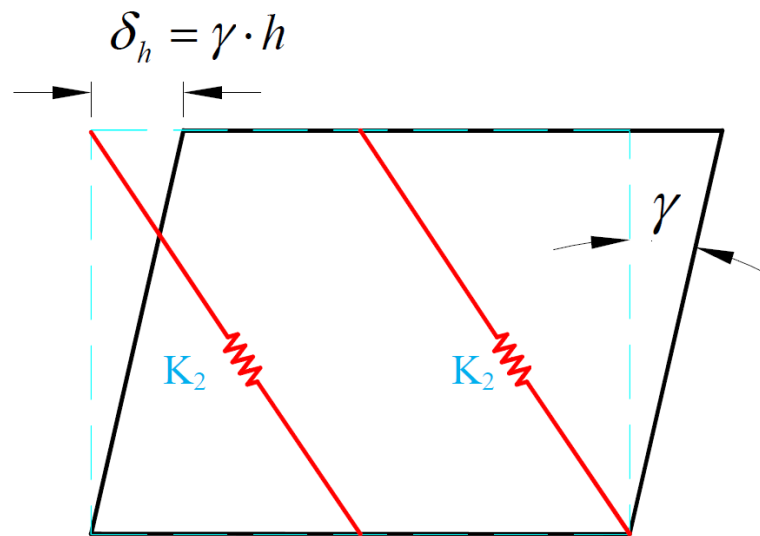
(a) K$_2$ Springs, in Parallel (Horizontally)
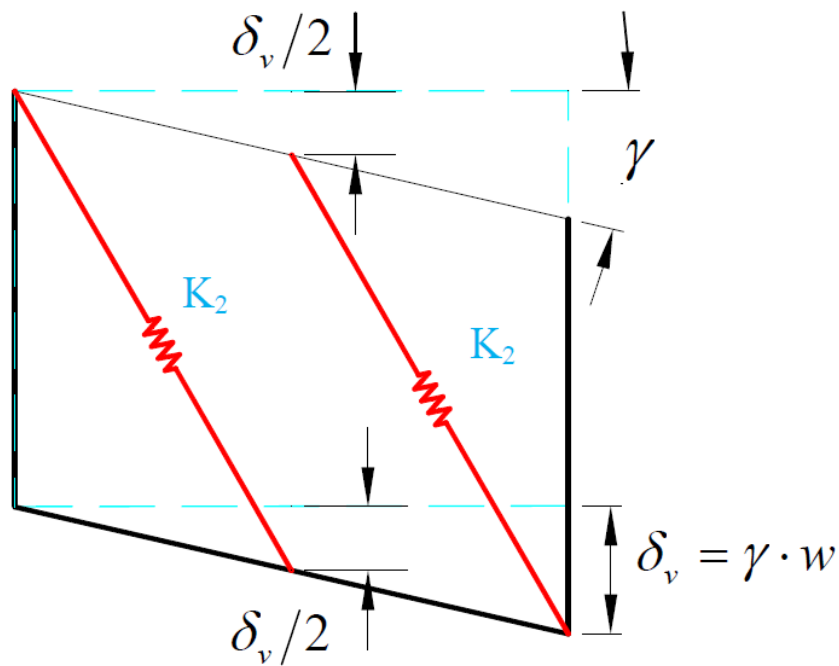


(b) K$_2$ Springs, in Series (Vertically)

Figure 3. 5. Type 2 Shear Springs in x and y Directions

Therefore, each Type 2 spring also has an anisotropic contribution to the shear stiffness of the macro-element, where the stiffness of each Type 2 spring in x and y directions will be K$_2$ and K$_2$/2, respectively; see Fig. 3-5. The non-orthogonal transformation matrix for the Type-2 springs is shown in Equation (3-9).

36

$$T_2 = \begin{bmatrix} C \cdot \sqrt{2} & -S/\sqrt{2} & 0 & 0 \\ S/\sqrt{2} & C \cdot \sqrt{2} & 0 & 0 \\ 0 & 0 & C \cdot \sqrt{2} & -S/\sqrt{2} \\ 0 & 0 & S/\sqrt{2} & C \cdot \sqrt{2} \end{bmatrix}$$

Eq. (3-9)

In which,

$$C = \cos(\theta_2), \quad S = \sin(\theta_2) \text{ and } \theta_2 = \arctan(2h/w)$$

Eq. (3-10)

The stiffness of all three types of springs is set to produce equivalent shear stiffness to the shear deformation produced by a pure shear element issuing a classic elastic material formulation, in both vertical and horizontal directions. While the total shear stiffness of the ten springs is set to produce the same shear stiffness as the classic formulation for a shear wall element, each shear spring type must be allocated percentage of the total shear stiffness separately. Based on the horizontal shear deformations, each pair of Type-1 springs are parallel to the equivalent spring pair on the other diagonal. Therefore, as the equivalent stiffness of each pair of Type-1 springs equals $K_1/2$, the final stiffness of both pairs will be equal to $K_1$. The total percentage of shear stiffness allocated to the Type-1 shear springs is 40 %. As all Type-2 shear springs undergo equal deformations horizontally and the total shear stiffness allocated to Type-2 springs is also 40 %, their stiffness will sum together, resulting in 10 % of the wall stiffness assigned to each of the four Type-2 shear springs. Finally, Type-3 shear springs also undergo equal deformations, and were thus each are assigned half of the allocated 20 % of the wall shear stiffness.

The resulting spring stiffnesses are shown in Equations 3-11 through 3-13. Equation 3-14 shows the equivalent shear wall stiffness for a shear wall element with the dimensions shown in Fig. 3-3-a.

$$K_1 = (0.4 \cdot K_{wall}) / (\cos(\theta_1))^2 \qquad \text{Eq. (3-11)}$$

$$K_2 = (0.4 \cdot K_{wall}) / (4 \cdot \cos(\theta_2))^2 \qquad \text{Eq. (3-12)}$$

$$K_3 = (0.2 \cdot K_{wall}) / (2 \cdot \cos(\theta_3))^2 \qquad \text{Eq. (3-13)}$$

In which,

$$K_{wall} = G \cdot w \cdot t / h \qquad \text{Eq. (3-14)}$$

$$\theta_1 = \arctan(h/2w)$$
$$\theta_2 = \arctan(2h/w)$$
$$\theta_3 = \arctan(h/w) \qquad \text{Eqs. (3-15)}$$

**Material model and Failure Criteria for Masonry Flexural and Shear Springs**

As is commonly assumed in a macro modeling approach [Zucchini et al., 2002], [Grecchi, 2010], [Flanagan et al., 2001], an isotropic homogeneous material behavior was assumed for the masonry in the proposed infill shear wall model. This is more consistent with the assumptions in the proposed macro-model and facilitates model calibration using a small number of material tests and design code defined material constants [Lourenço 1996].

Figure 3-6 shows the stress-strain behavior of a typical masonry assembly under tension and compression. As it can be observed in the figure, the masonry exhibits almost the same elasticity modulus in both tension and compression regions, although the nonlinear behavior is different [Lotfi et al. 1994]. Saneinejad and Hobbs [1995] suggested that, in compression, the secant stiffness of masonry infilled walls at the peak load is about half the initial stiffness. Thus, for the proposed masonry element in

38

this research, the secant elastic modulus at peak load, $E_{peak}$, is assumed to be half of the initial elastic modulus, $E_{initial}$ [El-Dakhakhni et al. 2004]. In addition, the nonlinear behavior of masonry walls was simplified using a tri-linear material model for compression and a bi-linear material model for tension as shown with thick dashed lines in Fig. 3-6. The strain at peak compressive stress, $\varepsilon_p$, was obtained from the tests, [Lumantarna et al. 2014]. Strains $\varepsilon_1$ and $\varepsilon_2$ are taken as approximate $0.5 \times \varepsilon_p$ and $1.5 \times \varepsilon_p$. The final strain, $\varepsilon_{final}$, was also assumed equal to 0.01. For an $\varepsilon_p$ of 0.002, the strains $\varepsilon_1$ and $\varepsilon_2$ will be 0.001 and 0.003, respectively, and thus defines the tri-linear material model for compression. This base material model is used for both flexural and shear masonry springs in compression.
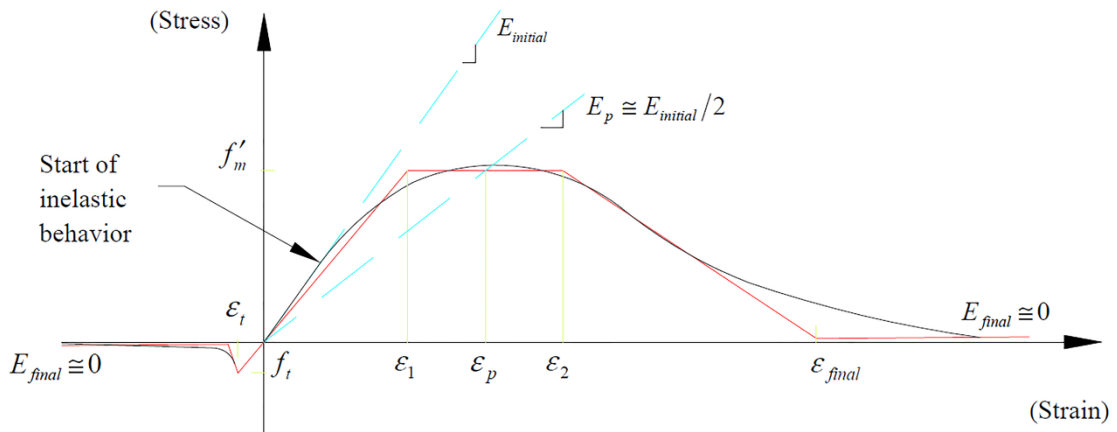


Figure 3. 6. Simplified Isotropic Material Model for Nonlinear Diagonal Shear and Flexural Springs

(Note: compression is shown in +y direction)

The tensile strength of masonry flexural springs was assumed equal to one tenth of compressive strength following the experimental tests of Lotfi et al. [1994]. The failure tensile strain was calculated as the tensile strength divided by the elastic modulus of the masonry.

Although the masonry is very brittle in tension, the masonry tensile behavior in flexure was modeled using a bi-linear material model as shown in Fig. 3-6. Typically, final tensile strains as low as the ones used by the proposed model can cause singularity problems in the analysis. However, the proposed model and analysis procedures are robust enough to preclude these singularity issues based on the fact that the model remained stable even with use of very low stiffness for the tensile springs.

The initial elastic modulus of the masonry, $E_m$, was set equal to the design code value (TMS 402-13/ACI 530-13/ASCE 5-13). For concrete masonry,

$$E_m = 900 \ f_m'$$

Eq. (3-16)

Where $f'_m$ is the specified compressive strength of masonry prism determined in accordance with the specification article 1.4 B.3 of TMS 602/ACI 530.1/ASCE 6 and [ASTM C1324].

As direct by the masonry code, the modulus of rigidity was assumed to be 40 % of the elastic modulus [MSJC 2013].

$$G_m = 0.4 \ E_m$$

Eq. (3-17)

To keep the modeling simple, the failure criteria proposed for flexural compression stress is also proposed for shear springs in compression. But, the tensile failure criterion for shear springs is slightly different from the tensile failure criterion of flexural elements.

The maximum allowable shear stress in unreinforced masonry shear wall elements described in the MSJC Masonry Design code [MSJC, 2013] is shown in Equation (3-

18) below. For the proposed shear wall model, it was conservatively assumed that each macro-element will start to fail at the same angular strain that a shear wall of equivalent dimensions and material properties reaches the allowable shear limits defined by the shear code limit. Thus, Equation (3-18) can then be used to determine the tensile failure criteria for the diagonal shear springs.

$$F_{vm} = \frac{1}{2}\left[\left(4 - 1.75\left(\frac{M}{Vd}\right)\right)\sqrt{f'_m}\right] + 0.25\frac{P}{A_n}$$ 
Eq. (3-18)

If it is conservatively assumed that there is no axial stress and the *M/Vd* ratio is at its largest value (1.0) required to be considered by code, then the allowable shear stress reduces to

$$F_{vm} = 1.125\sqrt{f'_m}$$ 
Eq. (3-19)

If the maximum permissible shear stress is set equal to the average applied shear stress, an angular (shear) failure strain, $\gamma_{vm}$, (tensile shear) can be determined as

$$\gamma_{vm} = \frac{F_{vm}}{G} = \frac{1.125\sqrt{f'_m}}{G}$$ 
Eq. (3-20)

In which, *G*, is the shear modulus of rigidity and *f'ₘ* is the compressive strength of masonry.

Under this angular strain, the change in the lengths of different types of springs can be determined using Equations (3-21-a) to (3-21-c). These spring length changes were then converted to strains as shown in Equations 3-22a through 3-22c. The relationship between the various strains and spring elongations are shown graphically in Fig. 3-7, as well.

Figure 3. 7. Angular Deformation of a Macro-Element and Strains Created in Each Spring Type

$$
\begin{aligned}
&L_1 = \sqrt{(H^2/4) + W^2} && , && \cos(\theta_1) = \frac{W}{L_1} && , && \Delta_1 = \frac{\gamma \cdot H}{2} \cdot \cos(\theta_1) \\
&L_2 = \sqrt{(W^2/4) + H^2} && , && \cos(\theta_2) = \frac{W}{2 \cdot L_2} && , && \Delta_2 = \gamma \cdot H \cdot \cos(\theta_2) \\
&L_3 = \sqrt{H^2 + W^2} && , && \cos(\theta_3) = \frac{W}{L_3} && , && \Delta_3 = \gamma \cdot H \cdot \cos(\theta_3)
\end{aligned}
$$

Eqs.(3-21-a-c)

$$
\begin{aligned}
&\varepsilon_1 = \frac{\Delta_1}{L_1} = \frac{\dfrac{\gamma \cdot H}{2} \cdot \cos(\theta_1)}{L_1} = \frac{\gamma \cdot H \cdot W/2}{(H^2/4) + W^2} \\
&\varepsilon_2 = \frac{\Delta_2}{L_2} = \frac{\gamma \cdot H \cdot \cos(\theta_2)}{L_2} = \frac{\gamma \cdot H \cdot W/2}{(W^2/4) + H^2} \\
&\varepsilon_3 = \frac{\Delta_3}{L_3} = \frac{\gamma \cdot H \cdot \cos(\theta_3)}{L_3} = \frac{\gamma \cdot H \cdot W}{H^2 + W^2}
\end{aligned}
$$

Eqs. (3-22-a-c)

For a given macro-element aspect ratio, the maximum of the three tensile strains will be used to define the onset of shear failure in the macro-element. Thus, this maximum will be used as the tensile shear failure strain (or onset of nonlinear behavior) for all three types of shear springs.

42

$$
\begin{cases}
\dfrac{H}{W} \leq \dfrac{\sqrt{2}}{2} & \rightarrow & \varepsilon_t = \varepsilon_2 \\[2mm]
\dfrac{\sqrt{2}}{2} \leq \dfrac{H}{W} \leq \sqrt{2} & \rightarrow & \varepsilon_t = \varepsilon_3 \\[2mm]
\dfrac{H}{W} \geq \sqrt{2} & \rightarrow & \varepsilon_t = \varepsilon_1
\end{cases}
\qquad \text{Eq. (3-23)}
$$

Using the above relationships it can be shown that, for elements with height to width ratios of less than $\sqrt{2}/2$, the Type 2 springs, and for aspect ratio equal to $\sqrt{2}/2$, Types 2 and 3 springs will simultaneously produce higher tensile strains than Type 1 springs. Similarly, for height to width aspect ratios of greater than $\sqrt{2}$, the Type 1, and for aspect ratios equal to $\sqrt{2}$, Types 1 and 3 springs will produce higher tensile strains than Type 2 springs. Finally, for height to width aspect ratios of between $\sqrt{2}$ and $\sqrt{2}/2$, the Type 3 springs will produce higher tensile strains than other two types. Using this analysis, one can roughly predict that the first shear crack orientation will be either along a line from the corner to mid-height or a line from the corner to mid-width, or along the diagonal, depending on the aspect ratio. In addition, for some element aspect ratios the shear spring model will imply that the shear crack will fall between the main diagonal spring and one or the other diagonal shear spring types. Moreover, the proposed methodology for calculating the strains occurring in different shear spring types can be extended to include more shear springs (four, five, or more) and improve the prediction for first crack location and orientation.

It is important to note that the proposed prediction of first shear crack orientation can be useful in predicting the behavior of perforated infill/shear walls, where the direction of first crack is very important with respect to the load distribution and on the performance of the perforated infill shear walls.

As with the flexural springs, initially the stiffness of the shear springs was assumed equal in both tension and compression. After tension cracking, the tensile stiffness was reduced but the compression stiffness was not changed. But, if compression softening occurred both tension and compression stiffness were reduced.

## Sliding Shear Springs

In an effort to capture shear friction behavior and possibly doweling action (in case of reinforcements), an additional group of springs was introduced into the macro-element. These (two) springs are located at the interface between adjacent macro-elements, or the base of the wall. Each of these two springs is assumed to produce half of the sliding stiffness associated with the corresponding interface they are attached to.

For unreinforced masonry shear walls, the sliding shear springs are assumed to exhibit a rigid-plastic behavior; i.e. the stiffness of each sliding spring is infinite before failure but reduced to near zero above sliding force levels. Note that spring stiffness cannot actually be set to zero since this will result in a singularity in the stiffness matrix and numeric instability. The stiffness was set to a value small enough to maintain stability but a have little effect on the force distribution. The sliding force was determined using a Mohr-Coulomb approach, a material cohesion strength, a coefficient of friction and the normal stress state.

For reinforced masonry walls, if the steel reinforcement crossing the sliding surface has not yielded, the sliding shear springs are assumed to follow a rigid-nonlinear-plastic behavior. The initial stiffness of the sliding springs can be assumed near infinite. After the sliding spring force reaches a limiting force, the element will start to slide along the interface. However, in a reinforced masonry wall steel reinforcement

44

crossing the interface will prevent further sliding by doweling action. At this point, the stiffness of the sliding shear springs will be defined by the behavior of the crossing dowels. Finally, if the steel bars yield, either under transferred shear force and/or under flexural forces, the stiffness of the sliding shear springs will reduce to near zero. In this investigation, sliding shear failure is assumed to happen only at the ground level, as this is typically the weakest interface with the highest loading.

The ultimate resistance of an interface subject to shear forces can be modeled by accounting for the mechanisms of adhesion and interlock, friction and dowel action, if present. Note that these mechanisms interact with each other and cannot be simply added to determine the ultimate capacity of the interface.

Based on the Fib Model Code equation for concrete structures, the ultimate shear stress at the reinforced interface resulting from the three mechanisms can be simply described as shown in Equation 3-24. [Fib Model Code, 2010].

$$\tau_u = \tau_c + \mu \cdot \left( \rho \cdot \kappa \cdot f_y + \sigma_n \right) + \rho \cdot \sqrt{f_y \cdot f_m'} \qquad \text{Eq. (3-24)}$$

In which, $\tau_c$ is the cohesion strength, $\mu$ is the friction coefficient, $\rho$ is the ratio of area of reinforcement to the area of the interface and $\kappa$ is the interaction factor defined as ratio of current tensile stress in the reinforcement to the yield strength of the reinforcement. $\sigma_n$ is the compressive stress applied normally to the interface, $f_y$ is the yield strength of the reinforcing bars and $f_m'$ is the compressive strength of masonry.

In the case of unreinforced masonry infill walls, the ultimate stress is usually limited to only adhesion/interlocking mechanisms and friction.

It is initially assumed that all of the sliding shear springs have a known and near infinite stiffness. At each increase in load, the displacements for the sliding springs can be found and the internal forces in these springs can be calculated. These forces can then be compared to a limiting force defined in Equation 3-25.

$$F_{\lim} = \left(\tau_c + \mu \cdot \left(\rho \cdot \kappa \cdot f_y + \sigma_n\right)\right) \cdot A_{CONTACT}$$

Eq. (3-25)

Where, $A_{CONTACT}$ is the contact area of interface, and the other parameters are defined as before. It should be noted that when calculating the friction part of limiting force, $F_{lim}$, the vertical stress includes vertical compressive stress applied to the interface plus the stress added by the clamping force of any steel tension reinforcement that cross the interface. If the summation of forces in the sliding springs at an interface reaches its limiting force, then the resultant stiffness of the sliding shear springs at that interface are softened. In the case where the wall is reinforced and the reinforcements crossing the interface have not yielded, the doweling action of the steel bars prevents the complete sliding failure of the interface. Conversely in URMs, when the summation of forces created in sliding springs reaches $F_{lim}$, the sliding shear springs will be assumed to respond plastically, with the resultant stiffness of the pair of sliding springs reduced to near zero [Fib Model Code, 2010]. Thus, the resultant stiffness is assumed to soften to near zero in URMs, and in presence of un-failed crossing reinforcement, is assumed to soften to a value equal to the total bending-resistance of the crossing steel bars divided by the current slip along the interface.

If rebar is present, the amount of force carried by the doweling action in the interface of the model can be calculated using Equation 3-26. [Fib Model Code 2010]

$$F_s = k_{2,\max} \cdot A_s \cdot \sqrt{f'_m} \cdot \sqrt{f_y} \cdot \sqrt{1 - \left(\sigma_s / f_y\right)^2} \cdot \sqrt{\left(S / S_{\max}\right)}$$

Eq. (3-26)

46

In which, $k_{2,max}$ is the interaction coefficient for flexural resistance at $S_{max}$ (smaller or equal to 1.6 for circular reinforcements). $S$ is the current slip (smaller or equal to $S_{max}$ ). $S_{max} \approx (0.1 \; to \; 0.2)d_s$, and $d_s$ is the diameter of a reinforcing bar equivalent to the areas of all reinforcing bars crossing the interface. These areas are proportionally reduced to reflect any inelastic behavior [Patnaik et al. 2003]. $A_s$ and $\sigma_s$ are the area and current tensile stress in the equivalent rebar, respectively. All other parameters are as defined before.

Equation 3-26 defines the force in the reinforcing bars produced by dowelling action. Therefore, if one divides this force by the current slip of the interface, the resultant stiffness of the interface springs can be defined. This value is the force required to make the interface slip by a unit value, which is consistent with the classic definition of stiffness. In addition, Equation 3-26 reduces the doweling action force as the tensile stress in the reinforcement increases. Indeed, the more the clamping force the reinforcing bars provide at the interface, the more the friction mechanism dominates over the doweling action.

Finally, if slip reaches $S_{max}$, the bending resistance of the steel bars is no longer available and the stiffness of sliding springs reduces to near zero. However, in large interface slip values, the kinking effect of reinforcement (or the parallel component of the tensile force of inclined crossing reinforcement) may come into play, as shown in Fig. 3-8 [Fib Model Code, 2010].
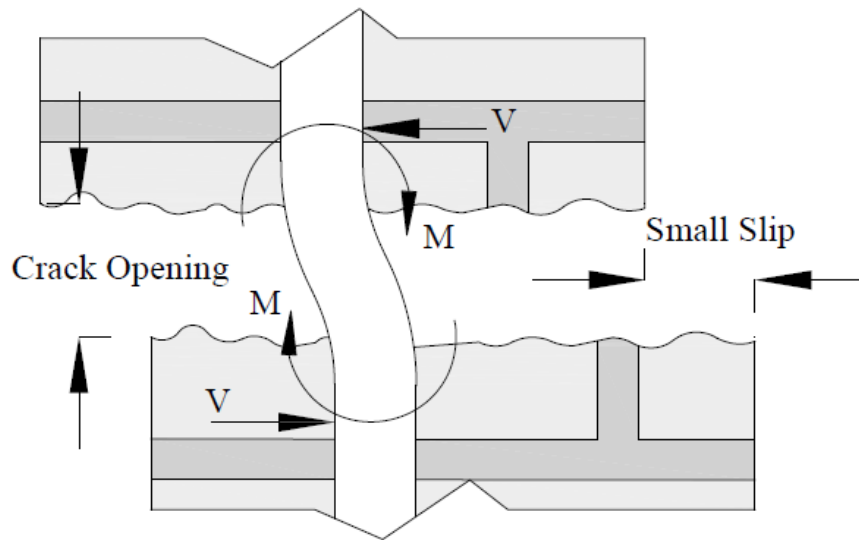
(a) Bending Effect
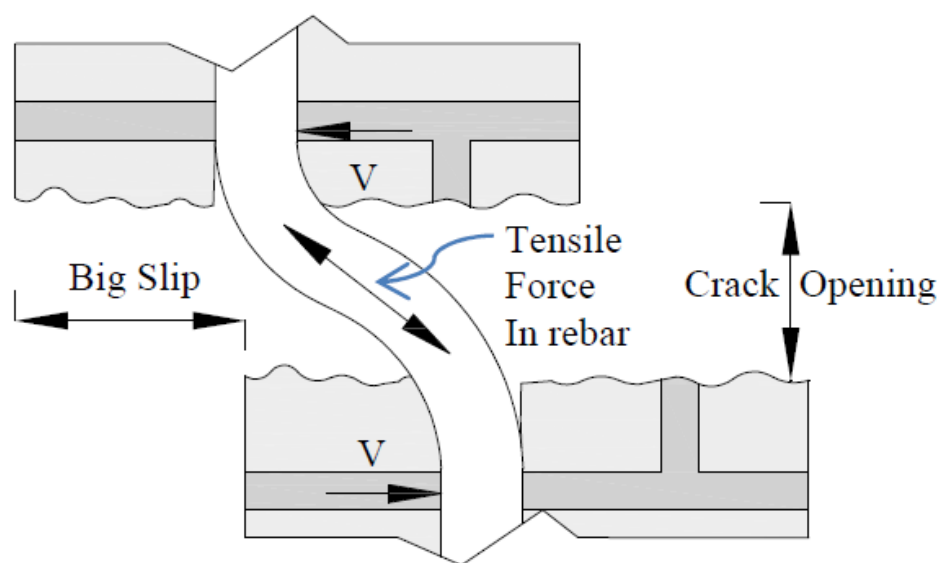


(b) Kinking Effect

Figure 3. 8. Doweling Action of Reinforcing Bar at Slip Interface

**Reinforced Masonry Infill Shear Walls**

In case of reinforced masonry infill shear walls, the macro-model needs to account for the effects of the reinforcing bars on the shear and/or flexure behavior. As mentioned earlier, participating reinforcing bars will be replaced by truss elements. In the

48

following sections, the procedures used to calibrate these reinforcing truss elements for shear and/or flexure will be discussed separately.

## Reinforcement Participation in Flexure

When a reinforcement crosses the interface between two contiguous macro-elements (usually perpendicular), it will affect the flexural behavior of the macro model. At each location where a bar is present an additional flexural element connecting the two contiguous rigid bars from two adjacent macro-elements is added. This new element behaves similar to the masonry flexural elements, with the exception that it will have one spring per reinforcement and the material model for the steel is consistent with conventional material models for mild steel. The stiffness of each spring is assumed to equal the tensile stiffness of the corresponding reinforcement; in order to simplify the problem for this research, it is assumed that the reinforcing bars are fully bonded with the surrounding masonry material. It is also important to mention that the length of the rebar can be different from the lengths of contiguous elements. See Fig. 3-9.
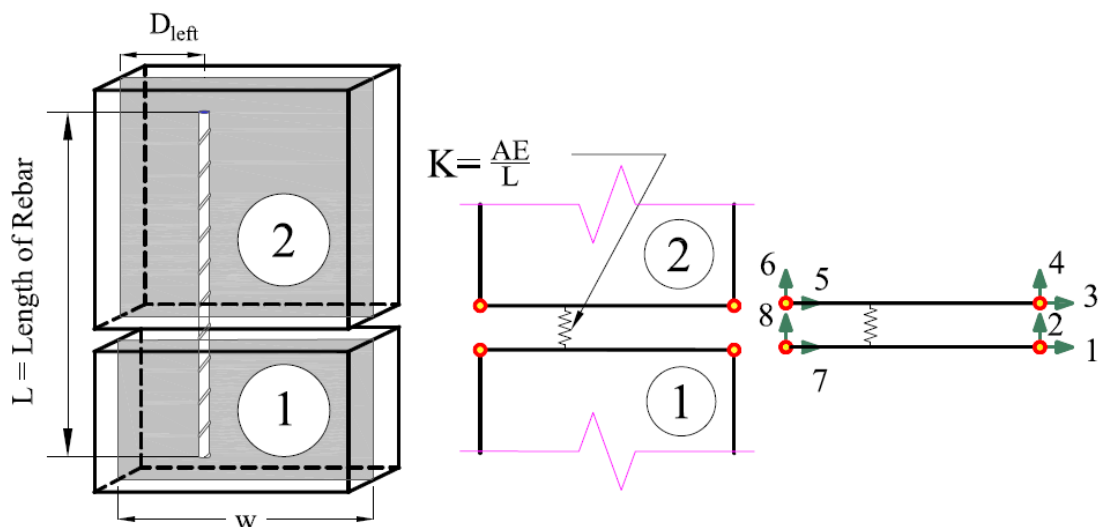


Figure 3. 9. Modeling the Reinforcements Participating in Flexure

In the following, the stiffness matrix of an interface with single crossing reinforcing bars is shown in Equation 3-27). This stiffness matrix can be easily extended to multiple reinforcing crossing the interface.

$$
K_{rebar\ in\ flexure} = \begin{bmatrix}
0 & 0 & 0 & 0 & 0 & 0 & 0 & 0 \\
0 & \varsigma & 0 & -\varsigma & 0 & -\xi & 0 & \xi \\
0 & 0 & 0 & 0 & 0 & 0 & 0 & 0 \\
0 & -\varsigma & 0 & \varsigma & 0 & \xi & 0 & -\xi \\
0 & 0 & 0 & 0 & 0 & 0 & 0 & 0 \\
0 & -\xi & 0 & \xi & 0 & \varsigma & 0 & -\varsigma \\
0 & 0 & 0 & 0 & 0 & 0 & 0 & 0 \\
0 & \xi & 0 & -\xi & 0 & -\varsigma & 0 & \varsigma
\end{bmatrix} \qquad \text{Eq. (3-27)}
$$

Where $\alpha$ and $\beta$ are defined as following.

$$
\varsigma = \frac{A_s \cdot E_s}{L_s} \cdot (D_{left}/w)^2 \qquad \text{Eq. (3-28)}
$$

$$
\xi = \frac{A_s \cdot E_s}{L_s} \cdot (D_{left}/w) - \alpha \qquad \text{Eq. (3-29)}
$$

**Reinforcement Participation in Shear**

The stiffness of equivalent truss elements are used for modeling steel  reinforcing bars obliquely crossing the macro-elements (such as horizontal shear reinforcing), to capture their effect on the shear deformation response of the masonry infill shear walls wall system. The shear steel truss element stiffness is calculated using the actual area and length of the steel reinforcing bars and its elastic modulus. Since shear reinforcing does not generally pass through the corners of the macro-elements chasses, the shear truss element stiffness matrix must be transformed twice to act in

accordance with the degrees of freedom defined at the corners of macro-elements. The stiffness matrix must be rotationally transformed to follow the direction of global degrees of freedom system and then mapped to the degrees of freedom defined at the corners of the macro-element chassis. The latter transformation matrix can be calculated using both the shape functions of a rectangular four-node isoparametric element and the location of points, in which, the reinforcement crosses the edges of macro-element chassis [Kwak and Filippou, 1997]. The global stiffness matrix of the aforementioned shear reinforcement truss element is given in Equation 3-30.

$$\left[K_{global}\right] = \left[T_2\right]^T \cdot \left[T_1\right]^T \cdot \left[K_{local}\right] \cdot \left[T_1\right] \cdot \left[T_2\right]$$

Eq. (3-30)

In which,

$$K_{local} = \frac{A_s E_s}{L_s} \begin{bmatrix} 1 & -1 \\ -1 & 1 \end{bmatrix}$$

Eq. (3-31)

And, the rotational transformation matrix, $[T_1]$, matrix is defined by:

$$[T_1] = \begin{bmatrix} \cos(\theta) & \sin(\theta) & 0 & 0 \\ 0 & 0 & \cos(\theta) & \sin(\theta) \end{bmatrix}$$

Eq. (3-32)

While $[T_1]$ can be simply computed using the angle $\theta$, created by the reinforcement and the positive direction of x-axis (see Fig. 3-10), $[T_2]$ varies if the reinforcement crosses the horizontal or the vertical edges of the macro-element. Equations 3-33 and 3-34 show the $[T_2]$ transformation matrices for the cases where the reinforcement either crosses the horizontal edges of the macro-element or the vertical ones, respectively.

51

$$[T_{2H}] = \begin{bmatrix} c_1/w & 0 & 0 & 0 & 0 & 0 & (1-c_1/w) & 0 \\ 0 & c_1/w & 0 & 0 & 0 & 0 & 0 & (1-c_1/w) \\ 0 & 0 & c_2/w & 0 & (1-c_2/w) & 0 & 0 & 0 \\ 0 & 0 & 0 & c_2/w & 0 & (1-c_2/w) & 0 & 0 \end{bmatrix} \qquad \text{Eq. (3-33)}$$

And,

$$[T_{2V}] = \begin{bmatrix} 0 & 0 & 0 & 0 & c_1/h & 0 & (1-c_1/h) & 0 \\ 0 & 0 & 0 & 0 & 0 & c_1/h & 0 & (1-c_1/h) \\ (1-c_2/h) & 0 & c_2/h & 0 & 0 & 0 & 0 & 0 \\ 0 & (1-c_2/h) & 0 & c_2/h & 0 & 0 & 0 & 0 \end{bmatrix} \qquad \text{Eq. (3-34)}$$

The angle $\theta$ along with dimensions $c_1$, $c_2$, $h$ and $w$ are shown in Fig. 3-10.
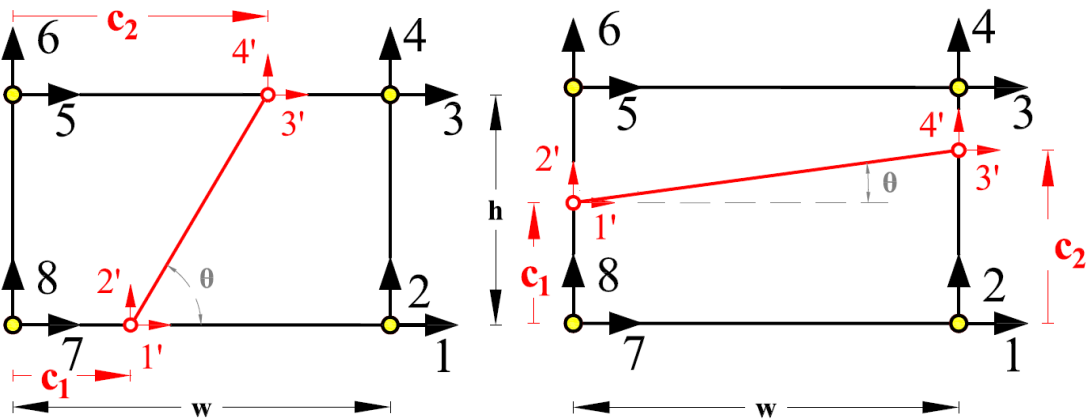


Figure 3. 10. Modeling of Reinforcement Participating in Shear

Although in this work, steel shear reinforcing bars are assumed to either cross the horizontal or vertical edges of the macro-element, the $[T_2]$ transformation matrix can be also computed for a combination of the two groups. More general crossing situations are addressed in the work of [Kwak and Filippou, 1997].

The effect of reinforcements in shear transfer (dowelling action) has been explained in detail in an earlier section.

52

# CHAPTER 4 : DISCUSSION

The previous sections described the proposed masonry shear wall macro-element. To test its robustness this element was subjected to a patch test. To evaluate the precision and efficiency of the proposed macro-model, it was used to predict the behavior of previously conducted experimental tests of masonry infill shear wall specimens. These tests included three unreinforced and two reinforced infill walls from work of [Dawe et al. 1989]. The results from the analytical models are then compared to the experimental tests to determine the accuracy and ease of use of the proposed infill masonry shear wall model.

In order to examine effect of different locations of openings in perforated infill shear walls, multiple models were created and analyzed under increasing lateral unidirectional loading (pushover analysis). The results of these analyses were compared to allow assessment of these effects and determine where openings should be encouraged and where they should be avoided. This chapter discusses each of these efforts in more detail.

**Patch Test of Proposed Macro Infill Masonry Shear Wall Element**

The patch test is a simple way for demonstration of the robustness of a given finite element. The test uses a partial differential equation on a domain consisting of several elements set up in a way that the exact solution is known. Typically, the exact solution consists of displacements, also known as constant strain solutions that vary following linear functions in space. An element will pass the patch test if the finite

element produces a solution that approaches the exact solution, as the mesh is refined. The origins of this test can be found in work of [Bruce Irons 1972]. Although, engineers have presumed for a long time that any element passing this test will necessarily converge to the exact solution if the mesh is refined enough, it was later found that it is not true. Researchers in late 1970s found that the patch test is neither necessary [Stummel 1980] nor sufficient [Sander et al. 1977] for convergence. Nonetheless, the quality of a new element can be examined by using this method as discussed below.

In any patch test process, the correct solution gives almost uniform conditions to which the patch is known to respond correctly, provided that the small perturbations from uniform conditions do not cause a disproportionate response in the patch. This condition is assumed by insisting that the stiffness matrix of the structural system is positive definite [Felippa, 2014].

To conduct the patch test, an unreinforced solid infill wall tested by Dawe et al [1989] was used. This test specimen (also considered in the numerical examples section) was analyzed using the proposed macro model shear wall elements with meshes of different sizes to evaluate whether the accuracy of the model will be increased, (converged to the single result) if finer mesh was used in modeling the infill wall. Again, the result of this test is neither adequate nor necessary to conclude that the finite element responses will converge to the correct answer ([Stummel 1980] and [Sander et al. 1977]) and the patch test is only used here to evaluate the quality of the proposed element and its robustness.

The shear wall test specimen incorporated an unreinforced masonry infill shear wall within a surrounding steel structural frame. The dimensions for the wall, concrete

blocks and frame members are shown in Table 4-1 while the material properties are provided in Table 4-2 [Dawe et al, 1989]. Note that the experimental test used 200x200x400 mm hollow concrete blocks (54 % Solid), but in the created macro-model "equivalent" solid concrete blocks of the same sizes are used to keep the geometry the same. This homogenization procedure significantly reduced the elasticity modulus of the equivalent concrete blocks in the model. The initial stiffness of the infilled frame given in the work of Dawe et al [1989] for each experimental test was used and back-calculated to get the modulus elasticity for homogenized solid concrete blocks for the corresponding macro-model. Using the elasticity modulus calculated by the aforementioned method, the compressive strength of the masonry assembly was calculated using the instructions of [MSJC 2013] for concrete masonry; see Equation 4.1.

$$E_m = 900 \cdot f'_m$$
Eq. 4-1

A unidirectional incremental pushover analysis was conducted on each of the models and Table 4-3, summarizes the approximate size of the meshes used to model the shear wall, along with the predicted maximum load and displacements.

Table 4. 1. Frame Dimensions and Cross Sections for Patch Test

| Frame Height (mm) | Frame Width (mm) | Columns' Cross Section (AISC – Metric.) | Beam's Cross Section (AISC – Metric.) | Concrete Blocks Dimensions (mm) |
|---|---|---|---|---|
| 2800 | 3600 | W250x58 | W200x46 | 200x200x400 |

Table 4. 2. Material Properties of Frame and Infill Wall considered in Patch Test

| Frame Material Properties | | | Infill wall Material Properties | | | |
|---|---|---|---|---|---|---|
| $E_s$ (psi) | $F_y$ (psi) | $F_u$ (psi) | f'$_m$ (for equivalent solid concrete blocks) (psi) | Cohesion Parameter (C) (psi) | Friction coefficient ($\mu$) | Special Weight ($\rho$) (lb/ft$^3$) |
| 29 x 10$^6$ | 4x 10$^4$ | 6x 10$^4$ | 512 | 150 | 0.7 | 135 |

Table 4. 3. Results of Patch Test

| Modeling Number | Number of Vertical Elements | Number of Horizontal Elements | Maximum Load Kips (kN) | Displacement at Ultimate Load inches (mm) |
|---|---|---|---|---|
| 1 | 2 | 3 | 130(578.3) | 0.788(20.0) |
| 2 | 3 | 4 | 113.7(504.7) | 0.807(20.5) |
| 3 | 4 | 5 | 107.3(477.2) | 0.811(20.6) |
| 4 | 5 | 6 | 104.7(465.7) | 0.811(20.6) |
| 5 | 6 | 7 | 104.3(464.1) | 0.815(20.7) |

The coarsest and finest meshing used in modeling numbers 1 and 5 of Table 4-3 are shown in Fig. 4-1.
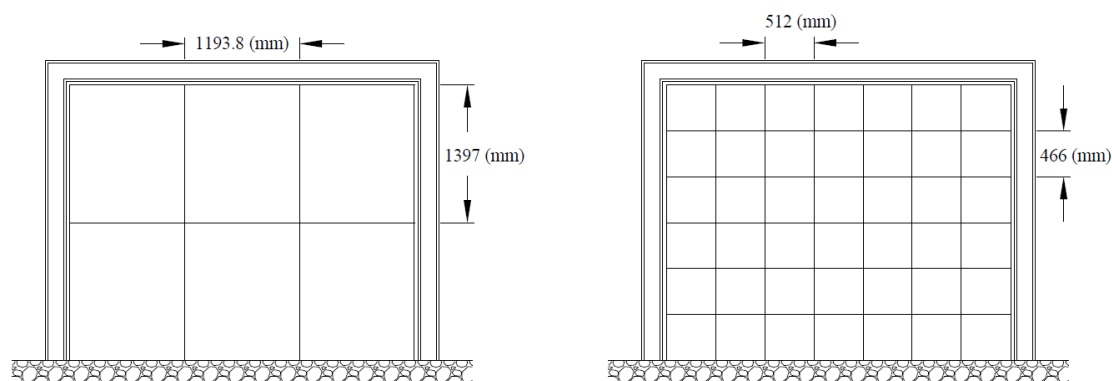


Figure 4. 1. Coarsest and Finest Meshing In Patch Test (NTS)

The Load-Displacement response for each of the analyses for each of the mesh sizes are shown in Fig. 4-2.
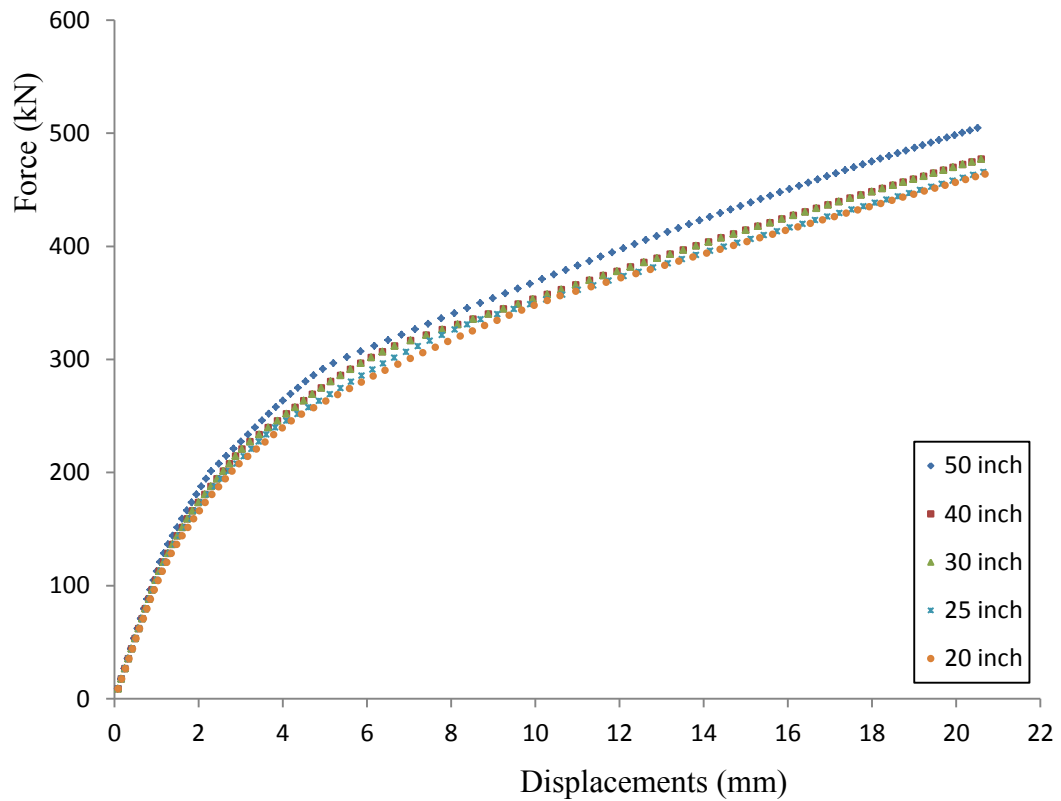


Figure 4. 2. Patch Test Results

Based on the results shown in Table 4-3, and the load-displacement equilibrium path diagrams shown in Fig. 4-2 for different mesh sizes, it can be concluded that the element has passed the patch test. This is reasoned because by refining the finite element mesh, the predicted answers approach to a constant value. In other words, after refining the average mesh size to 25 inches, additional refinement has little effect on the response of the model.

**Computer Program Implementation**

In this section, a brief description of the implemented program will be presented. In the first step, all specifications for frame and infill wall will be entered to the

program. The required specifications for frame and infill wall are presented in Tables 4-11 and 4-12.

Table 4. 4. Frame Elements and Reinforcements Specifications

| Specification | | Comments |
|---|---|---|
| Frame Height | | |
| Frame Width | | |
| Left Column | Left Column's Area | |
| | Left Column's Moment of Inertia | |
| Right Column | Right Column's Area | |
| | Right Column's Moment of Inertia | |
| Left Support Type | | |
| Right Support Type | | |
| Left Column to Beam Connection Type | | |
| Right Column to Beam Connection Type | | |
| Elasticity Modulus of Frame Members | | |
| $F_y$ of Frame Members | | Not Included in Model |
| $F_u$ of Frame Members | | Not Included in Model |
| Elasticity Modulus of Reinforcements | | |
| $F_y$ of Frame Members | | |
| $F_u$ of Frame Members | | |
| Special Weight of Frame Members | | |

Based on the geometric specifications entered as inputs to the program, the program first defines the meshing of the infill wall. In case of solid infill walls, the program first runs a patch test for different refinement of meshing in order to find the coarsest meshing size. For perforated infill walls, the model requires that at least a pair of macro-element to be considered along the distances between the opening and the frame members; the program then uses the size of these elements as an approximation of average element size for meshing. The program then assigns numbers to the degrees of freedom for frame members, macro-elements and supports.

The nonlinear stiffness matrices for different elements are computed as described briefly in the following sections. They are assembled together in order to calculate the total stiffness matrix of structure. Note that two-dimensional beam-column elements have been used for modeling the frame members.

Table 4. 5. Infill Wall Specifications

| Specification | | Comments |
|---|---|---|
| Order of Integration | | $2^{nd}$ Order Integration/$4^{th}$ Order Integration |
| Gap on Sides of Wall | | |
| Wall Height | | Distance From Ground to the Face of Beam Minus the Gap on Top of the Wall |
| Wall Width | | Distance Between the Internal Faces of Columns Minus the Sum of Gaps on Sides of the Wall |
| Wall Thickness | | |
| Openings Dimensions | Opening Height | |
| | Opening Width | |
| Openings Location | Door Opening | Horizontal Distance of Left Side of Door Opening from the Internal Face of Side of the Wall |
| | Window Opening | Horizontal and Vertical Distances of Left Bottom Corner of Window from the Bottom Left Corner of the Wall |
| Compressive Strength of | | |
| Cohesion Parameter | | |
| Friction of Coefficient | | |
| Special Weight of Masonry | | |

**Flexural Stiffness Matrix**

- For each flexural element

  - $(L_1 + L_2)$ = sum of lengths of panels

  - $\lambda$ = assumed fiber width

  - $\theta$ = angle between the rigid bars of element and +x axis

  - n = Number of springs in element (element width / $\lambda$ )

  - Define the DOFs of element

59

- [T] = Transformation Matrix
- For each spring in flexural element
  - $E_i$ = Elasticity Modulus of i$^{th}$ spring
  - $\varepsilon_i$ = Strain at i$^{th}$ spring
  o Modify the elasticity modulus of i$^{th}$ spring according to material model
  o Compute the flexural stiffness matrix of each element. (See Chapter 3)

**Shear Stiffness Matrix**

- For each wall panel
  - H = Height of the wall panel
  - W = Width of wall panel
  - Length of different spring types. (See Chapter 3)
- Define the failure criteria
  o in tension

$$\varepsilon_1 = \left(0.5 \cdot \gamma_{shear} \cdot H \cdot W\right) / \left(W^2 + H^2/4\right)$$  Eq. 4-2

$$\varepsilon_2 = \left(0.5 \cdot \gamma_{shear} \cdot H \cdot W\right) / \left(H^2 + W^2/4\right)$$  Eq. 4-3

$$\varepsilon_3 = \left(0.5 \cdot \gamma_{shear} \cdot H \cdot W\right) / \left(H^2 + W^2\right)$$  Eq. 4-4

$$\varepsilon_t = \max(\varepsilon_1, \varepsilon_2, \varepsilon_3)$$  Eq. 4-5

  o in compression

$$\varepsilon_c = f'_c$$  Eq. 4-6

- Calculate the strains in each spring
- Modify the elasticity moduli of springs according to material model

Note: if a spring is in tension use tensile elasticity modulus

Otherwise, use compressive elasticity modulus. (See Chapter 3)

- Calculate the shear stiffness matrix along each diagonal

  - For each type of spring in tension:

    o find the stiffness matrix of each spring type

    o calculate the corresponding transformation matrix

    o transform the local stiffness to the DOFs of the element

    o assemble it to accumulatively compute the stiffness matrix of the diagonal along the corresponding diagonal

  - For each type of spring in compression:

    o find the stiffness matrix of each spring type

    o calculate the corresponding transformation matrix

    o transform the local stiffness to the DOFs of the element

    o assemble it to accumulatively compute the stiffness matrix of the diagonal along the corresponding diagonal

For Type One springs on either of diagonals find $[K_{1(local)}]$ and $[T_1]$. (See Chapter 3)

$$\left[ K_1 {}_{\substack{Main\ or\ Secondary \\ diagonal}} \right] = [T_1]\left[ K_{1\ local} \right]\left[ T_1^T \right] \qquad \text{Eq. 4-7}$$

For Type Two springs on either of diagonals find $[K_{2(local)}]$ and $[T_2]$. (See Chapter 3)

$$\left[ K_2 {}_{\substack{Main\ or\ Secondary \\ diagonal}} \right] = [T_2]\left[ K_{2\ local} \right]\left[ T_2^T \right] \qquad \text{Eq. 4-8}$$

61

For Type Three springs on either of diagonals find [$K_{3(local)}$] and [$T_3$]. (See Chapter 3)

$$\left[ K_3 \atop {\text{\tiny Main or Secondary} \atop \text{\tiny diagonal}} \right] = [T_3] \left[ K_3 {\atop \text{\tiny local}} \right] [T_3^T]$$  Eq. 4-9

Note: Three stiffness matrices for each type of springs on either diagonal are added together and assembled for degrees of freedom at the ends of the corresponding diagonal.

$$\left[ K {\atop \text{\tiny Main or Secondary} \atop \text{\tiny diagonal}} \right] = \left[ K_1 {\atop \text{\tiny Main or Secondary} \atop \text{\tiny diagonal}} \right] + \left[ K_2 {\atop \text{\tiny Main or Secondary} \atop \text{\tiny diagonal}} \right] + \left[ K_3 {\atop \text{\tiny Main or Secondary} \atop \text{\tiny diagonal}} \right]$$  Eq. 4-10

The stiffness matrix of each macro-element at the location of DOFs on the corners of macro-element includes the stiffness of each diagonal at their corresponding DOFs.

### Sliding Shear Stiffness Matrix

Initially the stiffness matrix of the sliding shear springs are assumed equal to infinity. Under change in the applied loading, the forces calculated in each sliding shear spring is calculated and compared to the defined limiting force.

If the current force was greater or equal to the limiting force, the interface starts to slip.

- Following the occurrence of slip in the interface, if unreinforced, the stiffness of the sliding shear spring are reduced to near zero. It cannot reduce to zero as it creates singularity.

- Following the occurrence of slip in the interface, in the presence of reinforcements, it prevents further slips by dowel action.

    o The flexural force created in the reinforcement are calculated and divided by the current slip of the interface to calculate the new stiffness of the shear springs.

62

- By increasing the transferred shear load, if the force created in the reinforcements causes shear failure of the reinforcements or it fail in tension, the stiffness of sliding shear spring is reduced to near zero.

**Solution Method**

To analyze the models created in this research, an arc-length method was used [Felippa, 2014]. When using arc-length method, an initial big arc-length can be used provided that the structure behaves linearly at the beginning. Later, proportionally smaller arc-lengths are used as the structure degrades, which help capturing the behavior of the structural system. In such way, bigger load steps/displacements are used by the program while the structure experience linear behavior and when the structure starts experiencing nonlinear behavior, the arc-length is reduced to address the behavior, correctly. This method seems to be computationally efficient because even with finer meshing the computational effort remains low.

As mentioned before, in experimental work of Dawe et al [1989], the frame elements were kept in linear range, probably to be able to reuse the frames in other experiments. Worth to mention that to reach to the limit state in arc-length analysis method, all structural components should degrade such that the structure gradually becomes unstable. On the other hand, as the frame elements in the models in this research were assumed to remain elastic to match to what was reported in the experimental tests [Dawe et al 1989] because of the intact stiffness of frame members, the model was not able to degrade completely to reach to the limit state.

To address this issue in the model, for each infilled frame, the initial stiffness of total structure (frame and infill wall) was calculated at the first step. Then the stiffness of

frame structure (without the infill wall) was calculated. Through the analysis, the stiffness of frame structure was subtracted from the stiffness of total structure (frame and infill wall) to calculate the stiffness of infill-wall-Only. When the calculated stiffness degraded to a low percentage of the initial stiffness of the infill wall (1% for unreinforced and 2% for reinforced infill walls), it was assumed that the wall is totally failed leading to the limit state. In this moment, the program stops the analysis.

## Numerical Examples

### Unreinforced Masonry Infill Walls

In order to evaluate the accuracy of proposed model, three unreinforced masonry infill shear wall tests conducted by [Dawe et al, 1989] were modeled using the proposed macro-model and the predicted force-displacement responses were compared to those of measured for each of the tests. The tests were designated WA4 (a solid URM infill wall with no gaps in top and sides of the wall) and WC3 and WC5 (similar frames but with perforated infill walls). The WC3 test had a central opening of 800 mm by 2200 mm and the WC5 specimen contained the same opening but this opening was offset 600 mm from the center towards the loaded side. The height and width of frames in all three tests were 2800 and 3600 mm, respectively. The AISC Metric steel wide flange sections used for the columns and beams of the surrounding frames were W250x58 and W200x46, respectively. See Figs. 4-3 to 4-5. The geometric configuration of tests WA4, WC3 and WC5 are presented in Table 4-4.

Although, the masonry material models in the proposed macro-elements can be calibrated using the results of standard material tests, (such as compressive and a diagonal tensile tests) the initial linear portion of the measured load deflection

64

response was used to determine the elastic modulus of the masonry in the model. This was done to remove the inaccuracy of the material tests from the assessment of the model accuracy. Conventional elastic-plastic steel material models were used for the steel elements, including the reinforcing bars. The values for initial stiffness of the infilled frames were given in the experimental work of Dawe et al, [1989]. The elasticity moduli for frame members and the reinforcements are assumed to be the same but the frame members have been assumed to remain elastic through the analysis. It should be noted that partially grouted and hollow concrete masonry blocks (200 mm x 200mm x 400 mm) were used in the experimental tests [Dawe et al 1989], but to simplify the modeling, "equivalent" solid concrete blocks with lower elasticity modulus were assumed in the modeling process. The elasticity modulus of masonry wall was calculated based on the initial stiffness from the tests and the solid block assumption [Dawe et al 1989].
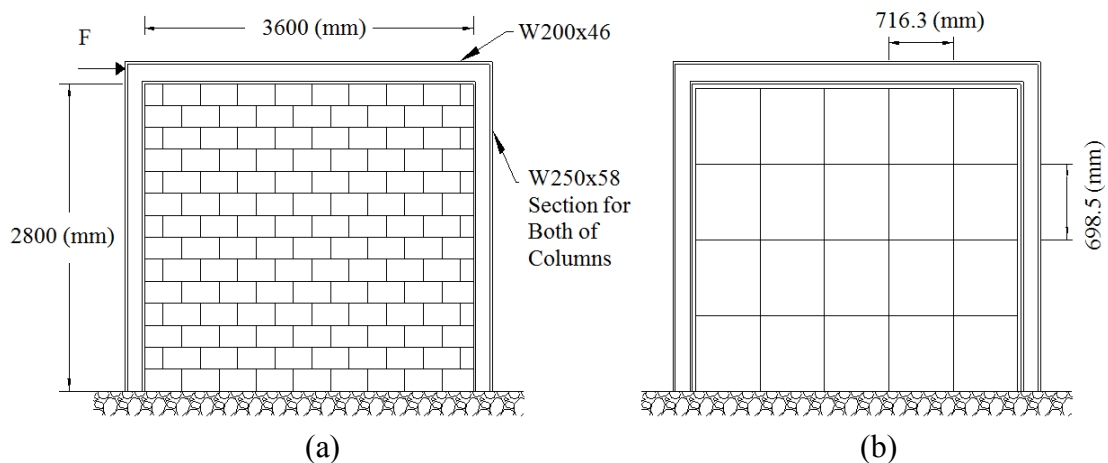


Figure 4. 3. WA4 Test
(a) Experimental Test (Solid Wall) [Dawe et al. 1989] ; (b) Proposed Macro-Model
Macro-Model For Infill Wall With Central Opening (NTS)
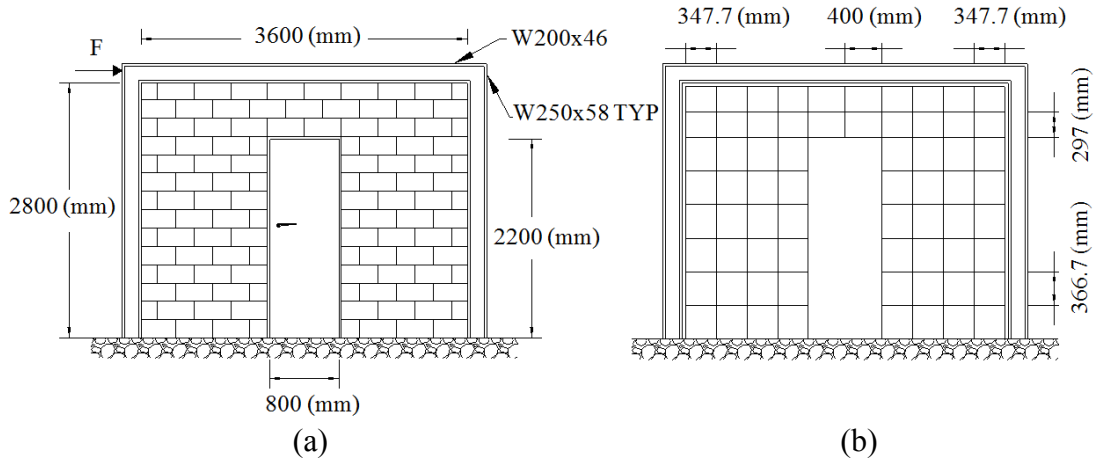
Figure 4. 4. WC3 Test

(a) Experimental Test (Central Door Opening) [Dawe et al. 1989]; (b) Proposed Macro-Model For Infill Wall With Central Opening (NTS)
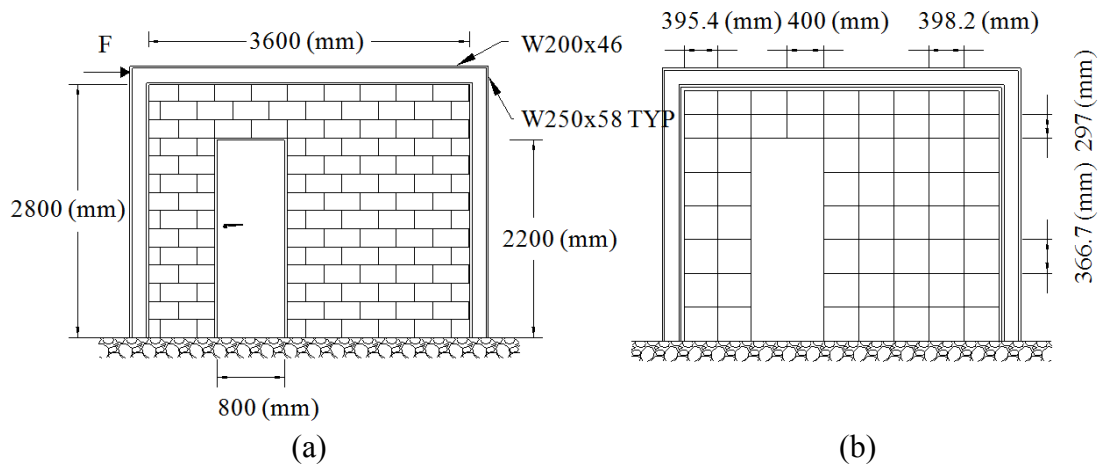


Figure 4. 5. WC5 Test

(a) Experimental Test (Door Opening Offset Towards the Loaded Side) [Dawe et al. 1989]; (b) Proposed Macro-Model For Infill Wall With Offset Door Opening (NTS)

Table 4. 6. Geometrical Specifications for WA4, WC3 and WC5 tests

| Test | Frame Height (mm) | Frame Width (mm) | Door Height (mm) | Door Width (mm) | Door Location | Column's Section (AISC-Metric) | Beam's Section (AISC-Metric) | Concrete Block size (mm³) |
|------|------|------|------|------|------|------|------|------|
| WA4 | 2800 | 3600 | -------- | ------- | -------- | W250x58 | W200x46 | 200x200x400 |
| WC3 | 2800 | 3600 | 2200 | 800 | Central | W250x58 | W200x46 | 200x200x400 |
| WC5 | 2800 | 3600 | 2200 | 800 | 600 mm Offset towards Loaded Side | W250x58 | W200x46 | 200x200x400 |

66

A monotonic incremental pushover load analysis was conducted on each of the models shown in Figures 4-3b through 4-5b. The macro element mesh for each infill wall was determined by keeping the number of the macro-elements small while maintaining approximately as square aspect ratio. For wall without openings little difference in performance was seen with even relative course meshing. For walls with openings, the most accurate response from the model was achieved when the shortest distance between the opening and edges of the wall determined the average mesh size. The meshing for perforated infill walls must be such that at least two macro elements are placed along the aforementioned distance. A finer mesh can be used but does not appreciably change the predicted wall performance

It should be noted that the elasticity modulus of each of the masonry infill walls models was derived from the measured initial stiffness of the infill walls for each of these tests [Dawe et al 1989], as only the initial stiffness of each of the tests was given in the published information. In addition, in the experimental tests, hollow 200x200x400 mm concrete masonry blocks were used. To simplify the modeling, "equivalent" solid masonry blocks were assumed during the macro-modeling process. This assumption required lowering the elasticity moduli for "equivalent" solid concrete masonry blocks to produce the same strength and stiffness as the hollow units. This homogenization process is consistent with the assumptions in masonry design code (MSJC), in which, the stresses and strains are assumed to be resisted by a homogenous masonry assembly and the strength and stiffness of hollow or partially grouted masonry is reduced in proportion to the grouted percentage.

The material properties for the steel frame members in all three tests are the same and are presented in Table 4-2. It should be noted that during testing [Dawe et al 1989], the wall displacements were been kept small to keep the steel frame elements in the

elastic stain range. The material model for frame members in the macro-models also assumed that the steel members remained elastic for all analyses conducted in this investigation. The material properties for steel and masonry used for the analyses for each of these test configurations are given in Table 4-5.

Table 4. 7. Material Properties for WA4, WC3 and WC5 tests

| | Frame Material Properties | | Infill wall Material Properties | | |
|---|---|---|---|---|---|
| Test | $E_s$ psi(Mpa) | $f'_m$ (for equivalent solid concrete blocks) psi(Mpa) | (C) Cohesion Parameter psi(Mpa) | ($\mu$) Friction coefficient | ($\rho$) Special Weight lb/ft$^3$ (N/m$^3$) |
| WA4 | 29 x 10$^6$ (2x10$^5$) | 512 (3.53) | 150(1.034) | 0.7 | 135(21206.81) |
| WC3 | 29 x 10$^6$ (2x10$^5$) | 276.45(1.91) | 150(1.034) | 0.7 | 135(21206.81) |
| WC5 | 29 x 10$^6$ (2x10$^5$) | 317.11(2.19) | 150(1.034) | 0.7 | 135(21206.81) |

Figures 4-6 to 4-8 show the comparison of the force-displacement response predicted for each macro-model and those obtained experimentally for infill walls WA4, WC3 and WC5, respectively. Ultimate experimentally measured and computationally predicted force and displacements are summarized in Table 4-6, along with the differences between the two.

68
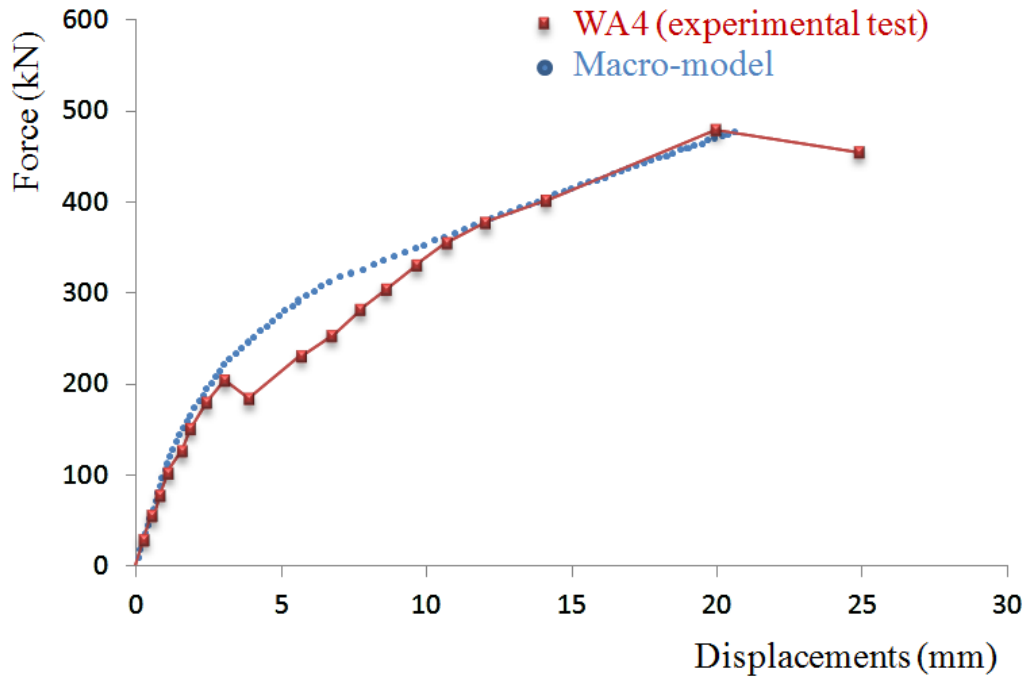
Figure 4. 6. Solid Infill Wall (WA4)

Experimental (data from [Dawe et al. 1989]) vs. Macro-Model
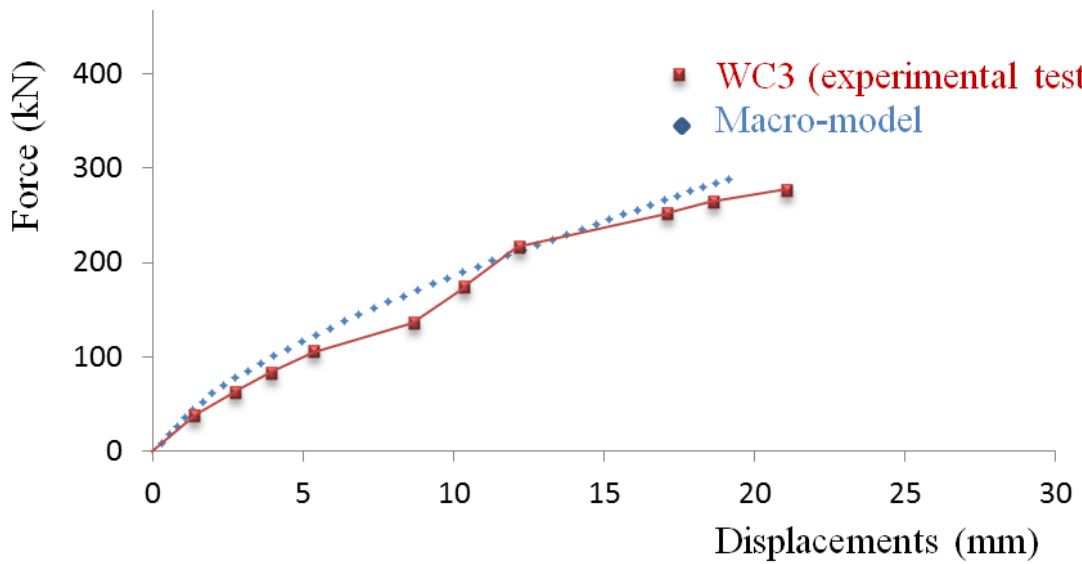


Figure 4. 7. Infill Wall with Central Opening (WC3)

Experimental (data from [Dawe et al. 1989]) vs. Macro-Model

69
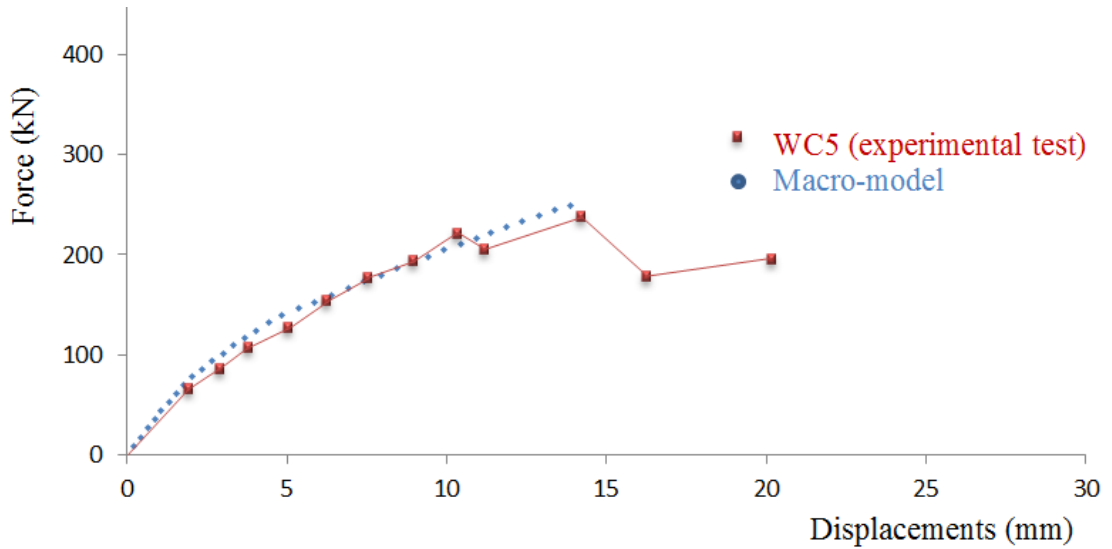
Figure 4. 8. Infill Wall with Opening Offset Toward the Loaded Side (WC5)

Experimental (data from [Dawe et al. 1989]) vs. Macro-Model

Table 4. 8. Experimental Test Results vs. Macro-model Results

| Test Name | Experimental Test | | Macro-Model | | Force Error (%) | Displacement Error (%) |
|---|---|---|---|---|---|---|
| | $F_{max}$ (kN) | $\Delta_{max}$ (mm) | $F_{max}$ (kN) | $\Delta_{max}$ (mm) | | |
| WA4 | 476 | 20.2 | 477.25 | 20.6 | 0.262 | 1.98 |
| WC3 | 285 | 21 | 288.72 | 19.14 | 1.31 | -8.85 |
| WC5 | 245 | 14.2 | 249.47 | 13.88 | 1.82 | -2.25 |

Note: $F_{max}$ = ultimate load; $\Delta_{max}$ = displacement at ultimate load on the equilibrium path

Examination of Figs. 4-6 through 4-8 and Table 4-6 shows that the macro-model was able to predict the force-displacement response of the tested walls with acceptable precision. In addition, the ultimate loads for all three models are predicted very accurately with the maximum error of 1.82 % for WC5 test. The ultimate displacements for WA4 and WC5 tests are predicted with a reasonable error. The error on the prediction for ultimate displacement of the WC3 test appears larger (less than 9 %), but Fig. 4-7 shows that the tangent stiffness of experimental test between the load points just preceding the ultimate load is very low and thus there is a large

70

increase in displacement for a very small increase in the load. If the measured loading point just prior to the peak loading point is compared to the predicted load response, a much closer agreement between measured and predicted performance is shown. Comparing the modes of failure predicted by the macro model with that shown in the tests shows that for WA4 test, the model predicts the first tensile crack on the lower left side of the wall where the tensile stress is the highest and then predicts shear cracks perpendicular to the compressive diagonal of the wall (note that these cracks were also tensile shear cracks). As the infill shear wall was confined by the steel frame, these tensile failures did not soften the structural model, significantly. Along with increase in the load, a local interface failure was observed in the element(s) where there were complete tensile failure (at lower left of the wall) and finally the ultimate load was reached just before a local compressive corner crushing was observed in the lower right side of the infill wall. In overall, the random shear cracks perpendicular to the compressive diagonal of the masonry shear wall were the most degrading failure type predicted by the model; and, the tensile failures predicted on the lower left side of the masonry shear wall and even local separation of the wall from the ground were not significantly reducing the stiffness of the system. In the experimental test also, the random shear cracks were reported as the main reason for degradation of shear wall and other failure modes were found to be not very effective. [Dawe et al 1989]. The macro model predicted the failure types, location and load acceptably close to the measured responses.

The first tensile crack appeared in the model WC3 test specimen, under a load lower than that measured experimentally. However, these were minor flexural tensile cracks, which were followed by a local element separation failure. Major shear cracks were predicted by the model at about the same load level as observed in the tests.

Note that in both the model and test these shear cracks did not significantly reduce the wall capacity. Finally, the model, predicts a slight local corner crushing of masonry on the lower right corner of the wall followed by major sliding failure in ground level of both sides of the infill wall. Sliding was observed in the test, although the corner crushing was not.  It should be noted that the corner crushing observed in the model was minor and very local.

Failure of the wall in the model for the WC5 wall specimen started with a major flexural tensile crack forming below the left side of the wall (the section adjacent to the loaded column). This crack was followed by diagonal shear crack on the right side of the opening (about ½ way up the pier). Immediately after the tensile shear cracks occurred in the right side of door opening, a local element separation failure happened on the left side (at the base of the pier). The interesting point about this wall was that the left side of the door opening did not experience a shear failure but just before the ultimate load, minor corner crushing happened in the lower right corner of the pier located to the left of door opening. It appeared that pier to the left of door opening was acting primarily in flexure. This behavior was similar to that observed in the experimental test for WC5 wall. In experimental WC5 test, evident sliding failure was reported similar to what predicted by the model; in addition, some minor (not through) diagonal cracks were also reported in the pier to the right side of the opening.

In general, the proposed macro-model was able to capture the failure modes and sequence observed in the experimental tests and was able to predict the ultimate load and the displacement at with an acceptable degree of accuracy.

## Reinforced Masonry Infill Shear Walls

In order to evaluate the accuracy of the proposed model for the case of reinforced masonry infill walls, two of reinforced masonry infill shear wall tests, conducted by Dawe et al, [1989] were analyzed using the proposed macro-model. The predicted and measured responses were then compared. The two test specimens were identified as WC4, WD5 [Dawe et al, 1989]. The WC4 specimen is a perforated reinforced masonry infill shear wall with no gaps on top or sides of the wall. The specimen had a central door opening of 800 mm by 2200 mm. A pair of 15M bars were used to form a lintel spanning the opening. The WD5 specimen was the same as WC4 with the exception of two additional 20M reinforcing bars were placed vertically on each side of the opening. The height and width of the frame in both tests was 2800 and 3600 mm, respectively and W250x58 and W200x46 (AISC -Metric) wide flange sections were used for the columns and beam elements, respectively. All infill walls were constructed with partially grouted 200 mm x 200mm x 400 mm concrete masonry units. See Figs. 4-9 and 4-10.
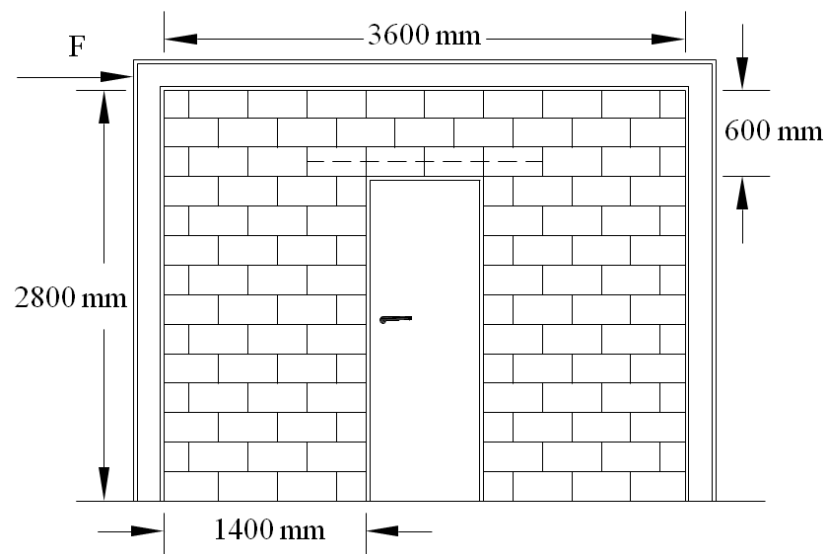


Figure 4. 9. WC4 Experimental Test (Perforated Infill Wall With Horizontal Reinforcements Only)  [Dawe et al. 1989] (NTS)

73
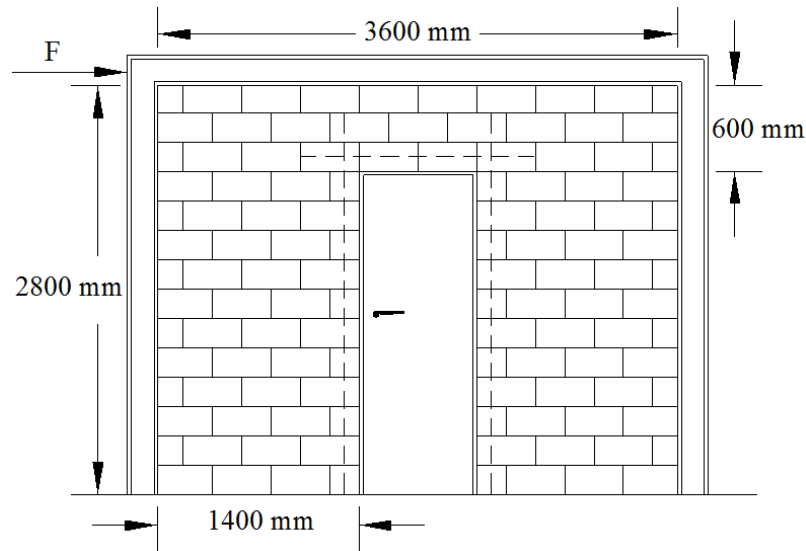
Figure 4. 10. WD5 Experimental Test (Perforated Infill Wall With Horizontal and Vertical Reinforcements) [Dawe et al. 1989] (NTS)

Although, the masonry material models in the proposed macro-elements can be calibrated using the results of standard material tests, (such as compressive and a diagonal tensile tests) the initial linear portion of the measured load deflection response was used to determine the elastic modulus of the masonry in the model. This was done to remove the inaccuracy of the material tests from the assessment of the model accuracy. Conventional elastic-plastic steel material models were used for the steel elements, including the reinforcing bars. The values for initial stiffness of the infilled frames were given in the experimental work of Dawe et al, [1989]. The meshing used for modeling WC4 and WD5 tests are exactly the same as the meshing used for WC3 test in the section for unreinforced masonry infill shear walls; see Fig. 4-4. The elasticity moduli for frame members and the reinforcements are assumed to be the same but the frame members have been assumed to remain elastic through the analysis. It should be noted that partially grouted and hollow concrete masonry blocks (200 mm x 200mm x 400 mm) were used in the experimental tests [Dawe et al 1989], but to simplify the modeling, "equivalent" solid concrete blocks with lower elasticity modulus were assumed in the modeling process. The elasticity modulus of masonry

wall was calculated based on the initial stiffness from the tests and the solid block

assumption [Dawe et al 1989].

The material properties of the frame members, masonry walls and reinforcement for

tests WC4 and WD5 are given in Table 4-7.

Table 4. 9. Material Properties Used for WC4 and WD5 Specimen Analyses

| Test | $F_y$ Steel Reinf. psi(Mpa) | $F_u$ Steel Reinf. psi(Mpa) | $E_s$ psi (Mpa) | f'$_m$ (for equivalent solid concrete blocks) psi (Mpa) | (C) Cohesion Parameter psi (Mpa) | ($\mu$) Friction coefficient | ($\rho$) Special Weight lb/ft$^3$ (N/m$^3$) |
|------|------|------|------|------|------|------|------|
| WC4 | 6x 10$^4$ (413) | 9x 10$^4$ (620) | 29 x 10$^6$ (2x10$^5$) | 276.45 (1.9) | 150 (1.034) | 0.7 | 135 (21206.81) |
| WD5 | 6x 10$^4$ (413) | 9x 10$^4$ (620) | 29 x 10$^6$(2x10$^5$) | 447.2 (3.08) | 150 (1.034) | 0.7 | 135 (21206.81) |

Figs. 4-11 and 4-12 show the force-displacement response predicted by the model for

an incremental unidirectional pushover analysis and measured for tests WC4 and

WD5, respectively. The experimental and computationally predicted force and

displacements peak values are presented in Table 4-8; in addition, errors in prediction

of ultimate forces and corresponding displacements are calculated and shown in a

separate column of the table.

75

Figure 4. 11. Infill wall with Central Opening (WC4)

Experimental [Dawe et al, 1989]) (red) vs. Predicted by Macro-model Analyses
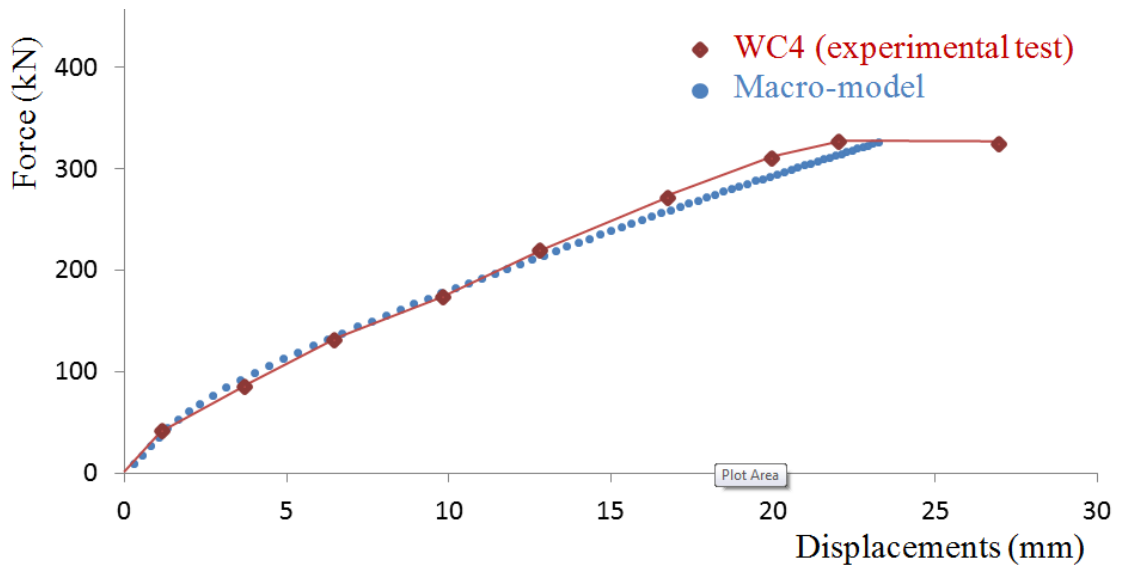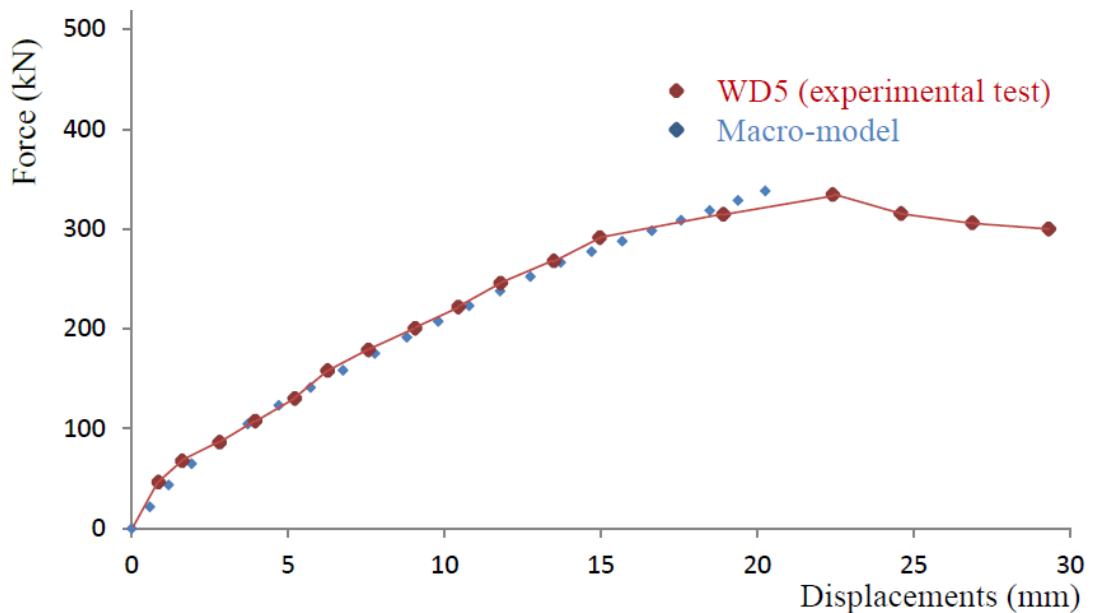


Figure 4. 12. Infill wall with Central Opening (WD5)

Experimental [Dawe et al, 1989]) vs. Predicted by Macro-model Analyses

As you can see in Table 4-8, the macro-model was able to predict the force-

displacement response of the reinforced masonry infill shear wall test specimens with

a reasonable degree of accuracy; the ultimate loads predicted for WD5 and WC4 were

76

within three percent of the measured values. The peak displacements for WC4 and WD5 tests are estimated to within less than two and ten percent error, respectively. Although the model slightly underestimates the ultimate displacement for the WD5 test, its estimation for ultimate load is reasonably close

Table 4. 10. Comparison of Experimental and Macro-model Predicted Results

|  | Experimental | | Macro-model | | Error | |
|---|---|---|---|---|---|---|
| Test Name | $F_{max}$ (kN) | $\Delta_{max}$ (mm) | $F_{max}$ (kN) | $\Delta_{max}$ (mm) | Force Prediction Error (%) | Displacement Prediction Error (%) |
| WC4 | 334 | 22.1 | 325.85 | 23.24 | -2.44 | 5.15 |
| WD5 | 335 | 22.2 | 338.01 | 20.01 | +0.92 | -9.61 |

Note: $F_{max}$ = ultimate load; $\Delta_{max}$ = displacement at ultimate load

The first failure described in the analysis of the WC4 specimen model was a flexural tensile failure in the lower left side of the infill wall (left-loaded-pier). This failure was followed by a local sliding failure in the same area. Following the sliding failure on the loaded side of the infill wall, tensile shear cracks started to appear in pier to the right of the door opening. These tensile shear cracks significantly decreased the stiffness of the infill wall. Additional tensile shear cracking then occurred in the upper half of the pier to the left of the opening. Indeed, because of the local sliding failure in the lower part of the left pier, this pier did not contribute significantly to the shear resistance of the assembly after the sliding occurred. After these failures occurred, corner crushing was predicted in the lower right part of the right hand pier, followed by a complete sliding failure on the lower right pier at the ultimate load.

In general, the model was able to predict the failure types observed during the test of specimen WC4. Although the order of occurrence for different failure types observed

in the analysis seems reasonable, it was not possible to check the order of occurrence because the order of failure types is not clearly described in the experimental work of Dawe et al [1989]. The presence of horizontal reinforcing bars in the lintel on top of the door opening did not significantly improve the in-plane load performance of the infill wall. In the analysis of the WD5 specimen, the model predicts the start of degradation by a minor tensile failure in the lower left of the left pier.  This crack is followed by local element separation failures happened in the same area as the load was gradually increased. These local element failures were followed by tensile shear cracking throughout the right pier and in the upper section of the left pier. It should be noted that the local sliding failures in the left pier were confined to a single element and did not lead to sliding of the entire left pier because the vertical reinforcement to the left of the opening prevented further sliding by dowel action. The model then predicted minor corner crushing failure at the bottom of the right pier. As the load was further increased, the model predicted additional tensile shear cracks occurred in near mid-height of the right pier and the vertical reinforcement on the right of door opening yielded. Next, the model predicted additional tensile shear cracks  in the upper triangle portion of the left pier as well At the ultimate load there was minor corner crushing predicted along the compression diagonal of the left pier. Again because the experimental test results [Dawe et al 1989] did not clearly mention the order of occurrence for different failure types, it is not possible to check if the model was able to predict the order of failures correctly. However, in general the predicted failure modes were observed and the ultimate load and the displacement at the ultimate load are predicted with an acceptable degree of accuracy.

## Effect of Opening Location on Infill Masonry Shear Wall Response

### Unreinforced Cases:

In the following section, different positions for a door opening in masonry infill shear wall are investigated. The purpose of this analysis is to determine how opening location affects the ultimate strength of infill masonry shear walls and its load deflection response. It is worth mentioning that all masonry infills were assumed to have the same material properties, and all of the dimensions of the frame, wall and door openings were the same size. Thus the only variable in this part of study was the distances from the door openings to the inside face of the left column. The door opening size was assumed to be equal to the door opening size of perforated walls in the numerical examples section; i.e. 2200 mm high and 800 mm wide. See Tables. 4-9 and 4-10.

Table 4. 11. Geometrical Configurations for Location of Door Opening Models

| Frame Height (mm) | Frame Width (mm) | Door Height (mm) | Door Width (mm) | Column's Section (AISC-Metric) | Beam's Section (AISC-Metric) | Concrete Block size (mm$^3$) |
|---|---|---|---|---|---|---|
| 2800 | 3600 | 2200 | 800 | W250x58 | W200x46 | 200x200x400 |

Table 4. 12. Material Properties for Location of Door Opening Models

| Frame | Infill wall | | | |
|---|---|---|---|---|
| $E_s$ (psi) | Assumed f'$_m$ (psi) | (C) Cohesion Parameter (psi) | ($\mu$) Friction coefficient | ($\rho$) Special Weight (lb/ft$^3$) |
| 29 x 10$^6$ | 300 | 150 | 0.7 | 135 |

Different locations for door opening are distinguished by the distance between the left side of door opening to the inside face of left column. See Fig. 4-13. Note that the left distance equal to 54.76 inches defines a central door opening.
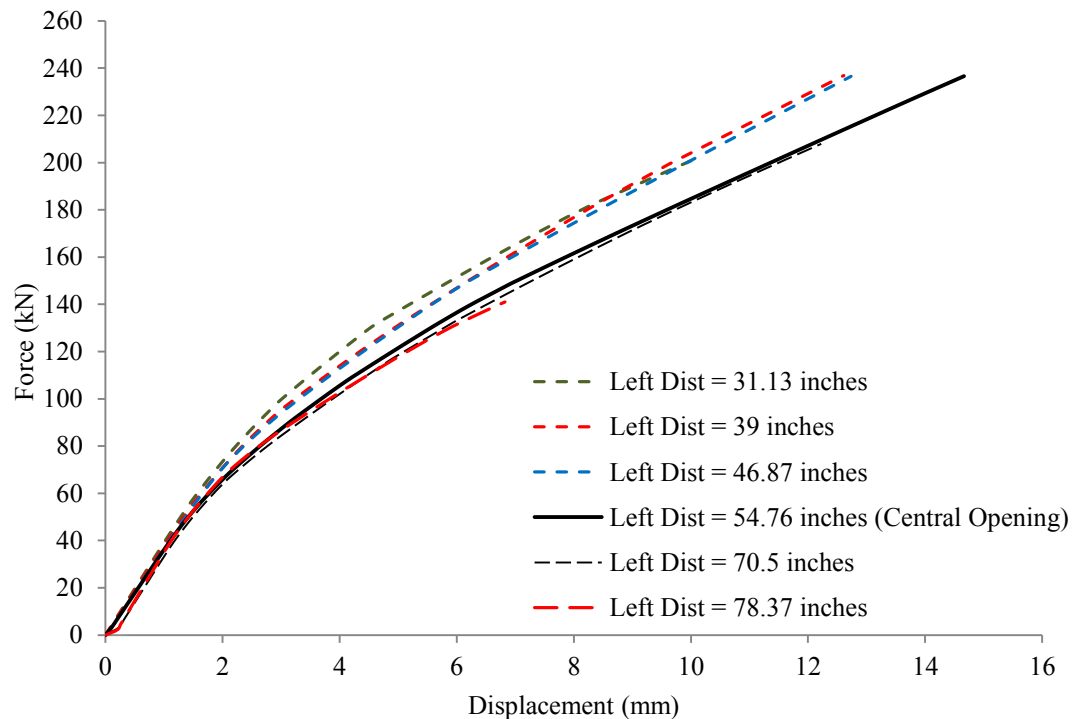


Figure 4. 13. Load-Displacement Responses for Different Locations of Opening

As it can be seen in Fig. 4-13, when the opening is central, the highest ultimate load resistance and most ductile behavior is predicted (shown by solid line). When the opening is offset from the center towards the loaded side, although the ultimate load is close to the ultimate load reached in the central case, the system shows much less ductility. On the other hand when the opening is offset from center away from the loaded column, the ultimate load reduces significantly. It can be concluded that a perforated infill wall will show the highest ultimate load and maximum ductility when the opening is central. A (central/ near central) opening will divide the infill shear wall to almost equal wall pier on each side of the opening, which help a more uniform load sharing due to their comparable stiffness. Thus, when one of the piers

80

experiences minor failures, the load share of its counterpart will increase only a small amount; this prevents sudden failure of the first panel, and a higher percentage of total capacity of the perforated masonry infill shear wall will be utilized.

### Reinforced Cases:

Reinforced perforated masonry infill shear walls are examined to assess the effects of opening location of the infill wall system performance. In the three configurations investigated, the frame size, shear wall and opening size were the same as those described for the unreinforced configuration. In addition there were three opening locations, one to the left of center, one with the opening centered in the shear wall length and one with the opening on the right side of center.  For all configurations, it was assumed that there were vertical 20M steel reinforcing bars on either side of the opening. In addition, a horizontal 20M reinforcing bar was extend across the masonry wall at the top of the opening and connected to both columns. Two, horizontal 20M reinforcing bars were also located at mid-height of the opening and connected through the  columns on both sides of the wall segment. See Figs. 4-14 to 4-16 for more detail.
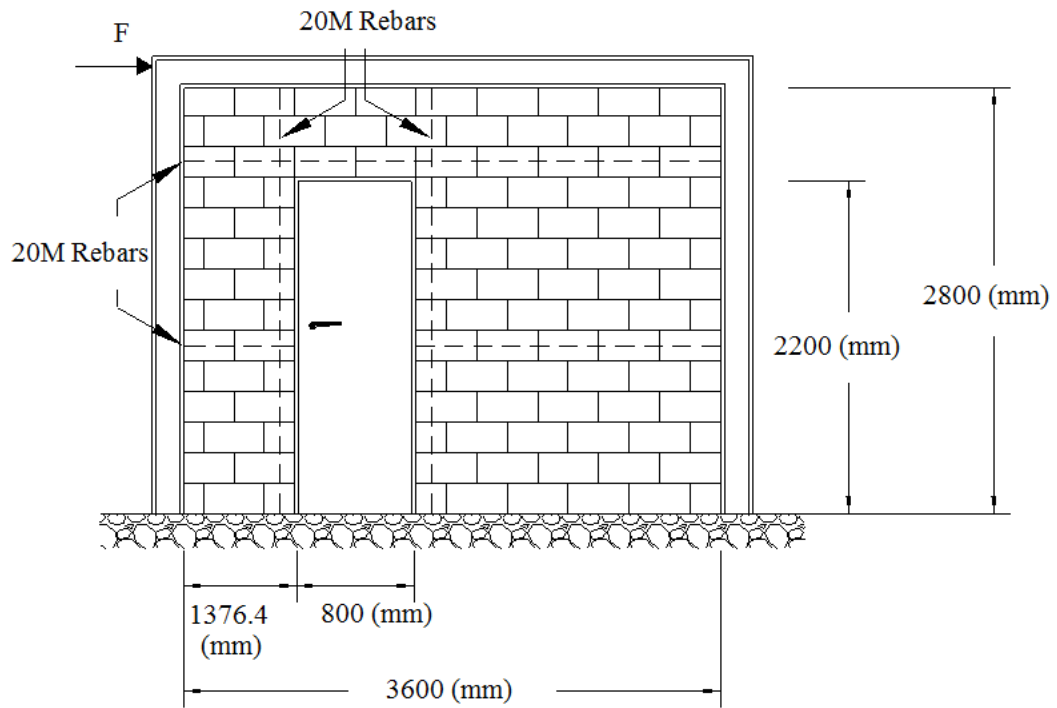
Figure 4. 14. Reinforced Infill Wall Case With Opening Offset Toward The Loading (NTS)

As it can be observed in Figs. 4-14 to 4-16, the percentage reinforcements for three examples with different locations of opening are exactly the same.
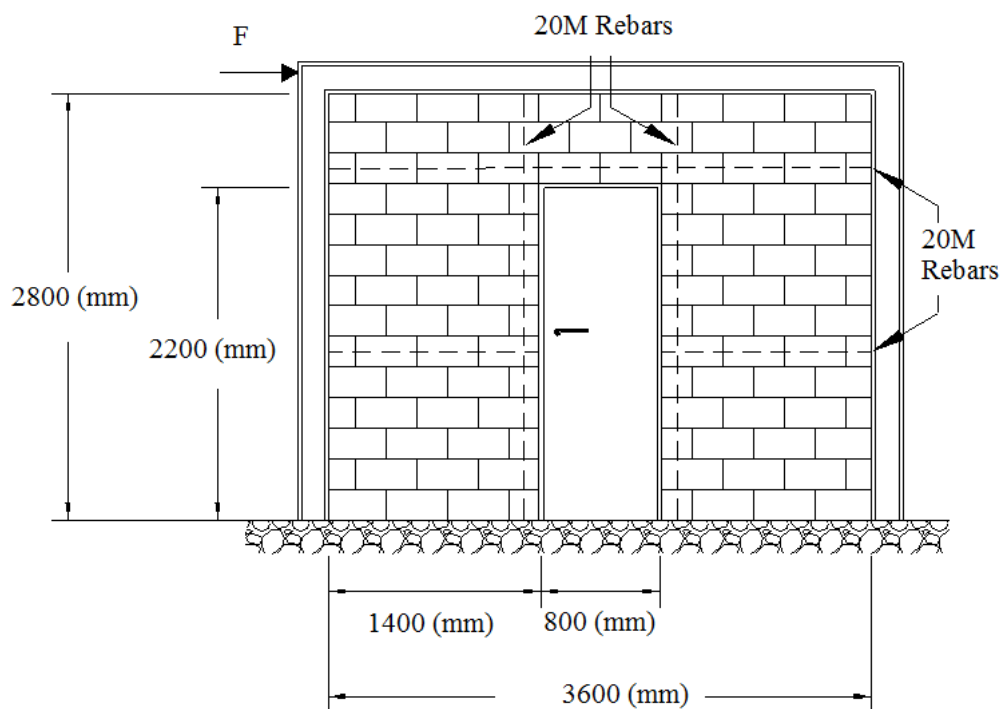


Figure 4. 15. Reinforced Infill Wall Case With Central Opening in Reinforced Infill Walls (NTS)

www.manaraa.com
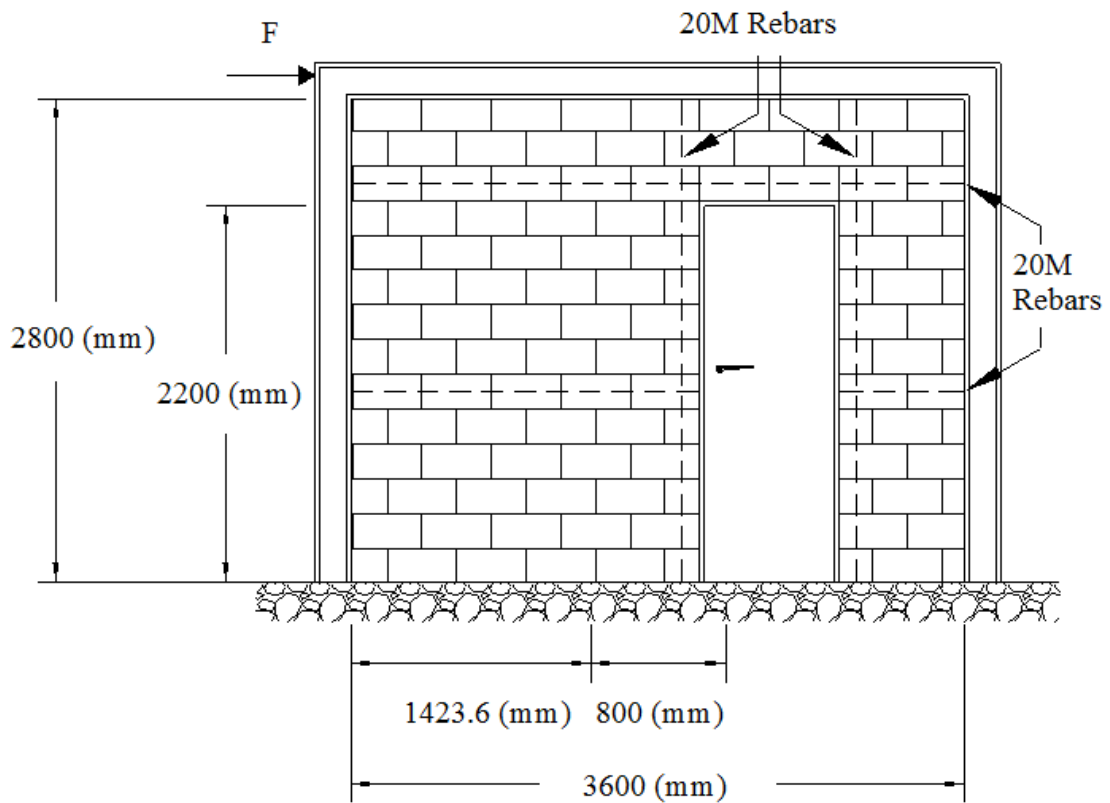
Figure 4. 16. Reinforced Infill Wall Case With Opening Offset Away From the Loading Reinforced Infill Walls (NTS)

For all three configurations, an incremental push over analyses was conducted and the predicted load-displacement response for the three perforated infill reinforced masonry shear walls are shown in Fig. 4-17.
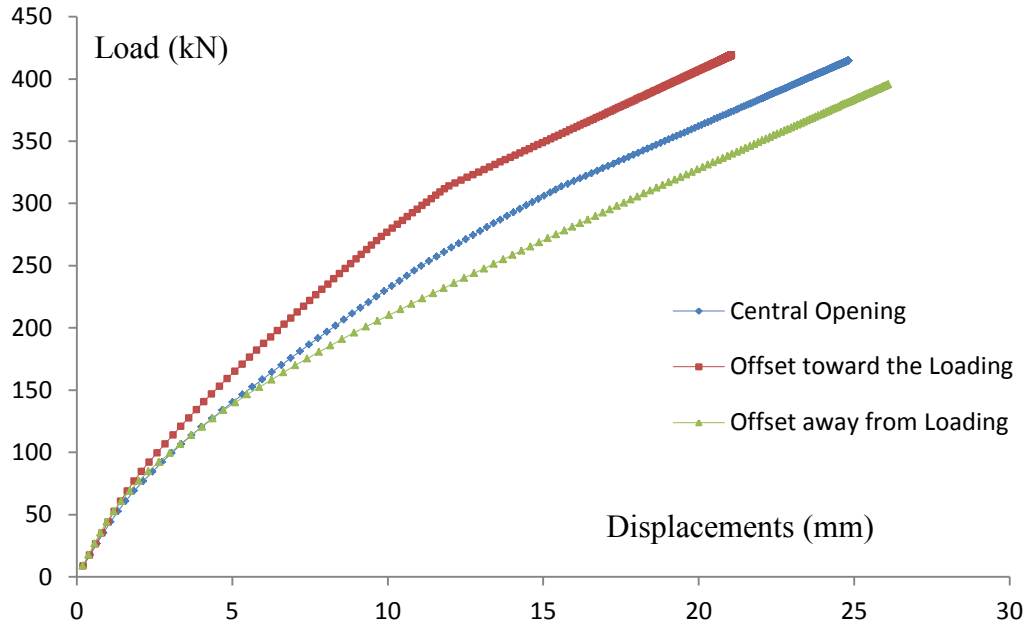
Figure 4. 17. Load-Displacement Diagrams For Reinforced Infill Walls With Openings

Figure 4-17 shows that the ultimate load of the reinforced infill wall with the opening offset towards the loaded side is higher than the other two cases, but the central opening case shows more ductility while the ultimate load is not much lower than the case where the opening is offset towards the loaded side.

**Effects of Openings - Summary**

Overall, the analytical models created to describe the response of masonry infill shear walls to study the precision of the model and evaluate the effects of openings on the response of infill masonry shear wall systems concluded that best performance for both unreinforced and reinforced perforated infill walls will be achieved if the door opening is located close to the centerline of the infill wall. In such cases, the overall structural system shows a higher ultimate load and more ductility under in-plane shear loading than other locations for the opening.

In addition, the analysis of the unreinforced masonry infill wall models suggest that openings offset away from the loading side reduce initial stiffness and ultimate system capacity. Thus, as these infill wall systems will undergo cyclic loadings under most lateral loadings, the best performance of the infill wall will be obtained if openings are located at or near the centerline of the infill wall.  This will produce the highest resistance and greatest ductility.

# CHAPTER 5: SUMMARY AND CONCLUSIONS

In many places around the world, masonry walls are enclosed by structural frame systems. In general, these structural systems can be categorized into two different groups; the first type, called nonparticipating infill shear walls, includes wall systems specifically constructed to avoid any interaction with the surrounding frame. The second category, known as the participating infill walls, includes walls that are intended to be in contact with the surrounding frame and thus contributory to the lateral resistance of the structure. Participating infill walls, will significantly affect the performance of the surrounding frame. This investigation concentrated on developing a method to predict the response of participating masonry infill shear walls.

As macro-models are simpler to use, do not need as much information to apply and are more computationally more efficient, this type of model was chosen for further consideration. Although many of the macro-models proposed hitherto fore for masonry infill shear walls were able to partially capture some of the behaviors observed in the infill wall systems under loading, none of the models was able to address all of the behaviors observed under simultaneous lateral and vertical loading. In addition, most of them could not address the effects of wall openings on the performance of the structural system nor the effect of reinforcements on the shear transfer mechanism.

After reviewing the properties of different wall models, an advanced macro-element infill shear wall model was developed based on the work of Caliò et al. [2012]. The proposed model has the following features:

86

1. A rigid bar chassis is created to form the boundaries of each infill masonry shear wall element.

2. Ten internal shear springs are used to capture the shear resistance of the wall instead of Caliò's pair of diagonal shear springs. This enables the model to degrade more gradually, better representing the actual behavior of the wall system.

3. The new model addresses the flexural stiffness using a closed form stiffness matrix based on a fiber-approach (flexural springs).

4. Springs are used to capture the shear transfer mechanism between the wall sections, including the dowel action of reinforced infill walls. Moreover, cohesion, friction and the doweling action of reinforcements crossing the interface between the elements was also considered in the defined interface shear transfer mechanism of the model using an interface shear spring.

5. The effect of reinforcements on shear and flexure in the cases where the infill wall is reinforced was addressed with steel spring elements.

6. Variable masonry elasticity moduli were used for flexural and shear springs. These variable moduli were set to allow the material to experience nonlinear behavior in tension while maintaining the compressive elasticity modulus at the same value. Thus, if the same spring goes into compression, e.g. under cyclic loading, the spring element can model compressive resistance while closing the tensile gaps under cyclic loading.

7. The variable elastic moduli were also set to degrade the tension response if significant inelastic compression strains were experienced. This models the condition where materials that have failed in compression show little or no resistance in tension.

87

8. Gap elements, the multiple constraints method and Lagrange Multipliers are used to account for gaps between the frame and wall, and the interaction between the two systems.

Procedures for calibration of each type of spring in the proposed macro-element were presented and are based on simple material tests and design code strength and stiffness relationships.

The proposed element and analysis procedures were applied to predict the behavior of five full sized tests on unreinforced and reinforced masonry infill walls confined by steel structural framing. Comparison of predicted and experimental behavior demonstrated that the proposed macro-model is able to predict the load-displacement equilibrium paths and estimate the ultimate loads and displacements of the experimental tests with an acceptable degree of accuracy.

In conclusion, the results of this research can lead to the following:

- The proposed macro-model was able to address different behaviors observed in the infill masonry shear wall systems including flexural, shear and shear transfer (sliding shear failure) using a rigid bar chassis, a variety of spring elements and variable material models to describe the in-plane load deflection behavior of unreinforced and reinforced infill masonry shear wall systems.

- The model can be easily calibrated by conducting a few code defined laboratory tests on small size masonry assemblages.

- A patch test on the proposed macro-element showed that same structure was modeled and analyzed repetitively using finer mesh sizes converge to a common answer and the model appears to be quite robust.

- When applying the model to full sized infill shear wall tests (unreinforced, reinforced and perforated) the computational models showed very good agreement with the experimental tests. Predicted ultimate strengths and deformations were quite close to measured values, generally within 5%. In addition the predicted failure modes were generally observed during testing.

- Assessment of the effects of perforations in the infill walls suggests that if these openings are located near or on the center-line of the infill wall, greater ductility of response and high ultimate resistances are expected.

### Recommendations for Future Work

Based on the result of his study the following additional work is recommended:

1. Although, the proposed macro-model was created in a way that it could address the cyclic behavior (Softened tension springs keep their compression stiffness but, softened compression springs lose their tensile stiffness), the model was used only to study monotonic incremental push over loading on different masonry infill walls. Thus, further studies should evaluate the proposed model under cyclic loading.

2. The current study limited itself to the analysis of bounding steel frame systems that remained elastic. The model should be evaluated where the bounding frame elements are either steel or concrete and where these elements that undergo significant inelastic deformation.

3. The current study was limited to single story systems. The proposed model should be evaluated for multistory applications.

4. The model should be evaluated for retrofit application where reinforcing may be surface applied, partially bonded.

5. The doweling action of reinforcement on the shear transfer mechanism was limited in the proposed model to the flexural resistance of the steel reinforcing bars. The model for doweling action of reinforcements could be extended to consider the kinking effect on the shear transfer interface when larger slips occur.

6. Further refinement of the failure mechanisms associated with the masonry infill wall is need to establish specific failure criterion so that a formalized code format design procedure can be developed.

# REFERENCES

Al-Chaar, G., Lamb, G.E., Abrams, D.P. (2003). "Effect of Openings on Structural Performance of Unreinforced Masonry Infilled Frames." *Proc. of 9<sup>th</sup>North American Masonry Conference*, Clemson University

Asteris, P. (2003). "Lateral Stiffness of Brick Masonry Infilled Plane Frames." *J. Struct. Eng.,* 10.1061/(ASCE)0733-9445(2003)129:8(1071)

Asteris, P., Antoniou, S., Sophianopoulos, D., and Chrysostomou, C. (2011). "Mathematical Macromodeling of Infilled Frames: State of the Art." *J. Struct. Eng.*, 10.1061/(ASCE)ST.1943-541X.0000384

ASTM C1324-10. (2010). "Standard Test Method for Examination and Analysis of Hardened Masonry Mortar." *ASTM International*, West Conshohocken, PA, 2010, www.astm.org

Balendra, T., and Huang, X. (2003). "Overstrength and Ductility Factors for Steel Frames Designed According to BS 5950." J. Struct. Eng., 129(8), 1019–1035.

Bashandy, T., Rubiano, N.R. Klingner, R.E. (1995). "Evaluation and Analytical Verification of Infilled Frame Test Data." *PMFSEL Report No. 95-1*

Bazan, E., and Meli, R. (1980). "Seismic Analysis of Structures with Masonry Walls." Proc., 7th World Conf. on Earthquake Engineering, Vol. 5, International Association of Earthquake Engineering (IAEE), Tokyo, 633–640.

Benjamin. H.R and Williams, H. A. (1958). "Behavior of One Storey Walls Containing Openings." *Journal of American Concrete Institute*, Vol. 30, No-5, Nov 1958, pp. 162-169.

Buonopane, S., White, R. (1999). "Pseudodynamic Testing of Masonry Infilled Reinforced Concrete Frame." *J. Struct. Eng.,* 10.1061/(ASCE)0733-9445(1999)125:6(578)

Caliò, I., Marletta, M., Pantò, B. (2012). "A New Discrete Element Model for the Evaluation of the Seismic Behavior of Unreinforced Masonry Buildings." *Engng. Struct.,* 40 (2012) 327–338

Caliò, I., Pantò, B. (2014). "A Macro-Element Modelling Approach of Infilled Frame Structures." *Computers & Structures*, 143:91–107, DOI: 10.1016/j.compstruc.2014.07.008

Chaker, A. A., and Sherifati, A. (1999). "Influence of Masonry Infill Panels on the Vibration and Stiffness Characteristics of R/C Frame Buildings." *Earthq. Eng. Struct. Dyn.*, 28(9), 1061–1065.

Chrysostomou, C. Z. (1991). "Effects of Degrading Infill Walls on the Nonlinear Seismic Response of Two-Dimensional Steel Frames." *Ph.D. thesis*, Cornell Univ., Ithaca, NY.

Chrysostomou, C. Z., Gergely, P., and Abel, J. F. (2002). "A Six-Strut Model for Nonlinear Dynamic Analysis of Steel Infilled Frames." *Int. J. Struct. Stab. Dyn.*, 2(3), 335–353.

Crisafulli, F. J. (1997). "Seismic Behaviour of Reinforced Concrete Structures with Masonry Infills.", *PhD Thesis,* Dept. of Civil Engng., Univ. of Canterbury, New Zealand, 416 pages

Crisafulli, F. J., and Carr, A. J. (2007). "Proposed Macro-Model for the Analysis of Infilled Frame Structures." *Bulletin of New Zealand Society for Earthq. Engng.,* Vol. 40, No. 2, June 2007

Dawe, J. L. and Seah, C. K. (1989). "Behavior of Masonry Infilled Steel Frames." *Canadian J. of Civil Engrng.,* 16, 865-876.

Durrani, A. J., and Luo, Y. H. (1994). "Seismic Retrofit of Flat-Slab Buildings with Masonry Infills." Proc., NCEER Workshop on Seismic Response of Masonry Infills, National Center for Earthquake Engineering Research (NCEER), Buffalo, NY.

El-Dakhakhni, W. W. (2002). "Experimental and Analytical Seismic Evaluation of Concrete Masonry-Infilled Steel Frames Retrofitted Using GFRP Laminates." *Ph.D. thesis,* Drexel Univ., Philadelphia, USA

El-Dakhakhni, W. W., Elgaaly, M., and Hamid, A. A. (2001). "Finite Element Modeling of Concrete Masonry Infilled Steel Frame." *9th Canadian Masonry Symp.,* National Research Council (NRC), Ottawa, Canada.

El-Dakhakhni, W., Elgaaly, M., and Hamid, A. (2003). "Three-Strut Model for Concrete Masonry-Infilled Steel Frames." *J. Struct. Eng.,* 10.1061/(ASCE)0733-9445(2003)129:2(177)

El-Dakhakhni, W., Hamid, A., Elgaaly, M. (2004). "Strength and Stiffness Prediction of Masonry Infill Panels." *13th World Conference on earthquake Engineering,* Vancouver, B.C., Canada August 1-6, 2004 Paper No. 3089

Fardis, M. N., and Calvi, O. M. (1994). "Effects of Infills on the Global Response of Reinforced Concrete Frames." Proc., 10th European Conf. on Earthquake Engineering, European Association for Earthquake Engineering (EAEE), Istanbul, Turkey, 2331–2336.

Fardis, M. N., and Panagiotakos, T. B. (1997). "Seismic Design and Response of Bare and Masonry-Infilled Reinforced Concrete Buildings. Part II: Infilled structures." J. Earthquake Eng., 1(3), 475–503.

Felippa CA., (2014) Introduction to Finite Element Methods, *Course Manual, ASEN 5007, http://www.colorado.edu/engineering/cas/courses.d/IFEM.d/* [6 June 2015]

FEMA 310. (1998). "Handbook for the Seismic Evaluation of Buildings." Federal Emergency Management Agency, Washington, D.C.

Fib Model Code for Concrete Structures. (2010), Fédération Internationale du Béton (fib), Lausanne, Switzerland

Flanagan, R. and Bennett, R. (2001). "In-Plane Analysis of Masonry Infill Materials." *Pract. Period. Struct. Des. Constr.,* 10.1061/(ASCE)1084-0680(2001)6:4(176)

Flanagan, R. D., and Bennett, R. M. (1999). "In-Plane Behaviour of Structural Clay Tile Infilled Frames." J. Struct. Eng., 125(6), 590–599.

Giannakas, A., Patronis, D. and Fardis M. (1987). "The Influence of the Position and the Size of Openings to the Elastic Rigidity of Infill Walls." *Proceedings of the 8th Hellenic Concrete Conference*, Xanthi, Kavala, Greece, pp. 49-56.

Grecchi, G. (2010). "Material and Structural Behavior of Masonry: Simulation with a Commercial Code." *Laurea Thesis*, University of Pavia., Lombardy, Italy, 2010.

Holmes, M. (1961)."Steel Frames with Brickwork and Concrete Infilling." ICE Proc., 19(4), 473–478.

IRONS, B.M. and RAZZAQUE, A., 1972, 'Experiences With the Patch Test for Convergence of Finite Elements", in *The Mathematical Foundations of* the *Finite Element Method with Applications* to *Partial Differential Equations,* Ed. Aziz, A. K., Academic Press, New York, 1972, p. 557.

Kakavetsis D.J., Karayannis C.G. (2009). "Experimental Investigation of Infilled Reinforced Concrete Frames with Openings." *ACI Struct. J.*, 03/2009, Vol. 106(No. 2):pp. 132-141

Klingner, R. E., and Bertero, V. V. (1978). "Earthquake Resistance of Infilled Frames." J. Struct. Div., 104(ST6), 973–989.

Kodur, V. K. R., Erki, M. A., and Quenneville, J. H. P. (1995). "Seismic Design and Analysis of Masonry-Infilled Frames." Can. J. Civ. Eng., 22(3), 576–587.

Kodur, V. K. R., Erki, M. A., and Quenneville, J. H. P. (1998). "Seismic Analysis of Infilled Frames." *Journal of Structural Engineering*, 25, 2, pp. 95-102, 1998-07-01

Kwak H.G. Filippou F.C. Nonlinear Finite Element Analysis of Reinforced Concrete Structures under Monotonic Loads 1990: *Rep*(*UCB/SEMM-90/14),*Univ.of Cal., Berkeley

Leuchars, J. M., Scrivener, J. C. (1976). "Masonry Infill Panels Subjected to Cyclic In-Plane Loading." *Bulletin of New Zealand National Soc. for Earthq. Engng.*, Vol. 9, No. 2, pp. 122-131

Liauw, T. C., and Lee, S. W. (1977). ''On the Behaviour and Analysis of Multi-Story Infilled Frames Subject to Lateral Loading.'' *Proc., Inst. Civ. Eng., Struct. Build.*, 63, 641–656.

Liauw, T.C. and Kwan, K.H. (1984). "Nonlinear Behaviour of Non-Integral Infilled Frames." *Comp. and Struct.*, 18, 551- 560, DOI: 10.1016/0045-7949(84)90070-1

Lotfi, H. and Shing, P. (1994). "Interface Model Applied to Fracture of Masonry Structures." *J. Struct. Eng., 10.1061/(ASCE)0733-9445(1994)120:1(63)*

Lourenço, P. B. (1996). "Computational Strategies for Masonry Structures." *PhD thesis*, Delft University, Netherlands

Lourenço, P. B., Roca, P., Modena, C., Agrawal, S. (Eds.). (2006). "Homogenization Approaches for Structural Analysis of Masonry Buildings." Struct. Analysis of Historical Constructions. *Proc. of the 5th International Conf*. New Delhi, India

Lumantarna, R., Biggs, D., and Ingham, J. (2014). "Uniaxial Compressive Strength and Stiffness of Field-Extracted and Laboratory-Constructed Masonry Prisms." *J. Mater. Civ. Eng.*, 10.1061/(ASCE)MT.1943-5533.0000731

Madan, A., Reinhorn, A., Mander, J., and Valles, R. (1997). "Modeling of Masonry Infill Panels for Structural Analysis." *J. Struct. Eng.*, 10.1061/(ASCE)0733-9445(1997)123:10(1295)

Mainstone, R. J. (1974). Supplementary Note on the Stiffness and Strengths of Infilled Frames, Building Research Station, Garston, UK.

Mainstone, R.J. (1971). "On the Stiffness and Strengths of Infilled Frames." *Proceedings of the Institution of Civil Engineers*, Supplement IV, 57-90

Mallick, D.V. and Garg, R.P. (1971). "Effect of Openings on the Lateral Stiffness of Infilled Frames." *Proc., Instn. Civ. Engrs.*, DOI: 10.1680/iicep.1971.6263 , 49(2):193-209

Mohebkhah, A., Tasnimi, A., Moghadam, H.A. (2007). "Modified Three-Strut (MTS) Model for Masonry-Infilled Steel Frames with Openings." *JSEE. Spring and Summer*, Vol. 9, No. 1,2/ 39

Mondal, G., Jain, S.K. (2008). "Lateral Stiffness of Masonry Infilled RC Frame with Central Opening." *Earthquake Spectra*, Vol. 24, N0.3, PP.701-723, Aug 2008

MSJC (Masonry Standards Joint Committee). (2013). "Building Code Requirements for Masonry Structures." *TMS 402-13,* Longmont, CO., /*ACI 530-13,* Farmington Hills, MI., /*ASCE 5-13,* Reston, VA

Park K.C. Felippa C.A. Gumaste U.A., A localized version of the method of Lagrange multipliers and its applications, *Comp. Mechs*, 24 (2000) 476±490 Springer-Verlag

Patnaik, S., Hopkins, D. (2003). *Strength of Materials: A New Unified Theory for the 21st Century*, Butterworth-Heinemann

Paulay, T., and Pristley, M. J. N. (1992). Seismic Design of Reinforced Concrete and Masonry Buildings, Wiley, New York, 744.

Polyakov, S. V. (1960). "On the Interaction Between Masonry Filler Walls and Enclosing Frame When Loading in the Plane of the Wall." Translation in earthquake engineering, Earthquake Engineering Research Institute (EERI), San Francisco, 36–42.

Reflak, J., and Fajfar, P. (1991). "Elastic Analysis of Infilled Frames Using Substructures." *Proc. 6th Canadian Conf. on Earthquake Engineering*, University of Toronto Press, Toronto, 285–292

Sander, G. and Beckers, P. - 'The Influence of the Choice of *Connectors* in the Finite Element Method', in *The Mathematical Aspects of the Finite Element Method,* Lecture Notes in Mathematics, Vol. 606, Springer-Verlag, Berlin, 1977, p. 316.

Saneinejad, A. and Hobbs, B. (1995). "Inelastic Design of Infilled Frames." *J. Struct. Eng.,* 10.1061/(ASCE)0733-9445(1995)121:4(634)

Smith, B. S. (1962). "Lateral Stiffness of Infilled Frames." J. Struct. Div., 88(6), 183–199.

Smith, B. S. (1966). "Behavior of Square Infilled Frames." *Journal of the Structural Division*, ASCE, Vol. 92, No.1, pp. 381-404

Smith, B. S., and Carter, C. (1969). "A method of Analysis for Infilled Frames." ICE Proc., 44(1), 31–48.

Stummel, F. - The Limitations of the Patch Test, Int. J. Numer. Meth. Engrg., 15, 177-188 (1980)

Syrmakezis, C. A., and Vratsanou, V. Y. (1986). "Influence of Infill Walls to RC Frames Response." Proc. 8th Europ. Conf. on Earthq. Engng., Lisbon 3, 6.5/47-53

Tassios, T. P. (1984). "Masonry Infill and RC Walls (An Invited State-Of-The- Art Report)." 3rd Int. Symp. on Wall Structures, Centre for Building Systems, Research and Development, Warsaw, Poland.

Thiruvengadam, V. (1985). "On the Natural Frequencies of Infilled Frames." *Earthquake Eng. Struct. Dyn.,* 13(3), 401–419

Utku, B. (1980). ''Stress Magnifications in Walls with Openings.'' *Proc., 7th World Conf. on Earthquake Engineering*, Vol. 4, Istanbul, Turkey, 217–224.

Zucchini, A. Lourenço, P.B. (2002). "A Micro-Mechanical Model for the Homogenization of Masonry." *Int. J. of Solids and Struct*. 39 (2002) 3233–3255

# CURRICULUM VITAE


## Farid Nemati
73, Charter Oaks dr.
Louisville, KY; 40241
(405)-437-8594
f0nema01@cardmail.louisville.edu

## Education

- **University of Louisville, Louisville, KY**
  **Structural Engineering**, Ph.D. Candidate,
  GPA (3.94); graduating by August 2015

- **Iran University of Science and Technology, Tehran, Iran**
  M.S. in **Structural Engineering**,
  Thesis Title: Symmetry in Space Structures
  GPA: 16.35 /20. Thesis Score 19.75/20

- **Bojnourd Azad University, Bojnourd, Iran**
  B.S. in **Civil Engineering**

## Technical Skills

- **Commercial Softwares**
    - Ansys
    - CSI softwares (SAP, Etabs, etc.)
    - Microsoft Office
    - AutoCAD
    - Formian Software, (for topology of space structures e.g. domes and barrel vaults)
    - STAAD and MicroStation

- **Programming**
    - Generating **Common and Specific Linear and Nonlinear Elements** practically used for FEA, in Matlab; e.g. *Gap-Contact Elements, Volumetric Elements, Layered Elements, etc.*
    - Creating **Nonlinear FEM Analytical Models** in Matlab for *Static, Dynamic and Stability problems* with *Graphical Representation* of the problem
    - Excel Spreadsheets

## Selective Graduate Coursework

- Advanced Finite Element Methods
- Advanced Structural Engineering
- Advanced Earthquake Engineering
- Advanced Design of Steel Structures

100

- Advanced Solid Mechanics
- Nondestructive Testing
- Structural Dynamics
- Timber Design
- Bridge Design

- Plastic Analysis and Design
- Project Management
- Stability of Structures
- Engineering Mathematics
- Statistical Data Analysis

## Published Journal Papers

- F. Nemati, A. Kaveh, **Eigensolution of rotationally repetitive space structures using a canonical form**, *Communications in Numerical Methods in Engineering*, DOI: 10.1002/ CNM.1265, 20 May2009.
- F. Nemati, A. Kaveh, **Efficient free vibration analysis of rotationally symmetric shell structures**, *Communications in Numerical Methods in Engineering*, DOI: 10.1002/ CNM.1318, August 2009.

## PhD Thesis Title

- MACRO MODEL FOR SOLID AND PERFORATED MASONRY INFILL SHEAR WALLS
- Papers are submitted for publication

## Work and Teaching Experience

- **Part time Structural Engineer:**
  Pardis Arian Saaze Consulting Corporation. Tehran, Iran; *2008-2010*
  Responsible for design of both Steel and Concrete Structures

- **Programming Skills:**
  **FEM programs** for Mechanical and Structural Engineers as a student at Iran University of Science and Technology; 2008-2009

- **Teaching Experience:**
  *Strength of Materials (I), Matrix Structural Analysis and Finite Element Method courses* at both undergraduate/graduate levels in Iran University of Science and Technology; 2007-2009

## Honors
- University of Louisville, Fellowship Award, 2011-2013
- Research Assistantship at Civil and Environmental Engineering Dept. 2013-now
- Rank 170 in the Iranian Nationwide University Entrance Exam among 25,000 participants, 2007